

1 A regional spatio-temporal analysis of large magnitude 2 snow avalanches using tree rings

3 Erich Peitzsch^{1,2*}, Jordy Hendrikx², Daniel Stahle¹, Gregory Pederson¹, Karl Birkeland^{3,2},
4 and Daniel Fagre¹

5 ¹ U.S. Geological Survey Northern Rocky Mountain Science Center, West Glacier, Montana, USA

6 ² Snow and Avalanche Lab, Department of Earth Sciences, Montana State University, Bozeman, Montana,
7 USA

8 ³ U.S.D.A. Forest Service National Avalanche Center, Bozeman, Montana, USA

9 [*epeitzsch@usgs.gov](mailto:epeitzsch@usgs.gov), 215 Mather Dr., West Glacier, MT, USA, 59936

10 **Abstract.** Snow avalanches affect transportation corridors and settlements worldwide. In many mountainous
11 regions, robust records of avalanche frequency and magnitude are sparse or non-existent. However,
12 dendrochronological methods can be used to fill this gap and infer historical avalanche patterns. In this study,
13 we developed a tree-ring based avalanche chronology for large magnitude avalanche events (size \geq
14 $\sim D3$) using dendrochronological techniques for a portion of the northern United States Rocky Mountains.
15 We used a strategic sampling design to examine avalanche activity through time and across nested spatial
16 scales (i.e. from individual paths, four distinct sub-regions, and the region). We analysed 673 total samples
17 from 647 suitable trees collected from 12 avalanche paths, from which 2,134 growth disturbances were
18 identified over years 1636 to 2017 Common Era (C.E.). Using existing indexing approaches, we developed
19 a regional avalanche activity index to discriminate avalanche events from noise in the tree-ring record. Large
20 magnitude avalanches common across the region occurred in 30 individual years and exhibited a median
21 return interval of approximately three years (mean = 5.21 years). The median large magnitude avalanche
22 return interval (3-8 years) and the total number of avalanche years (12-18) vary throughout the four sub-
23 regions, suggesting the important influence of local terrain and weather factors. We tested subsampling
24 routines for regional representation, finding that sampling eight random paths out of a total of 12 avalanche
25 paths in the region captures up to 83% of the regional chronology, whereas four paths capture only 43% to
26 73%. The greatest value probability of detection for any given path in our dataset is 40%, suggesting that
27 sampling a single path would capture no more than 40% of the regional avalanche activity. Results emphasize
28 the importance of sample size, scale, and spatial extent when attempting to derive a regional large magnitude
29 avalanche event chronology from tree-ring records.

30

31 **1 Introduction**

32 **1.1 Background**

33 Snow avalanches are hazardous to human safety and infrastructure (Mock et al., 2016; Schweizer, 2003) as
34 well as an important landscape disturbance affecting mountain ecosystems (Bebi et al., 2009). In the United
35 States an average of 27 people die in avalanche accidents each winter (CAIC, 2020). Avalanches, especially
36 large magnitude events, also affect transportation corridors and settlements throughout the world. For
37 example, avalanches impact numerous roadways and railroad corridors in the western United States
38 (Armstrong, 1981; Hendrikx et al., 2014; Reardon et al., 2008). Consequently, understanding general
39 avalanche processes and associated large magnitude avalanche return intervals is critical for local and
40 regional avalanche forecasters, transportation agencies, and land use planners.

41 Long-term, reliable, and consistent avalanche observation records are necessary for calculating avalanche
42 return intervals, which can be used in infrastructure planning and avalanche forecasting operations. However,
43 such records are often sparse or non-existent in many mountainous regions, including areas with existing
44 transportation corridors. Thus, inferring avalanche frequency requires the use of dendrochronological
45 methods to document damaging events or geomorphic response within individual trees at individual path to
46 regional scales. Even in regions with historical records, tree-ring dating methods can be used to extend or
47 validate uncertain historical avalanche records, which has led to the broad implementation of these methods
48 in mountainous regions throughout the world (e.g. Corona et al., 2012; Favillier et al., 2018; Schläppy et al.,
49 2014).

50 Numerous studies reconstructed avalanche chronologies in the United States using tree-ring methods
51 (Burrows and Burrows, 1976; Butler et al., 1987; Carrara, 1979; Hebertson and Jenkins, 2003; Potter, 1969;
52 Rayback, 1998). Butler and Sawyer (2008) provided a review of current methodologies and types of tree-
53 ring responses used in avalanche dendrochronological studies. Favillier et al. (2018) provided a more recent
54 comprehensive graphical summary of dendrochronological avalanche studies throughout the world.
55 Numerous studies used dendrochronological techniques to develop avalanche chronologies for remote
56 regions without historical avalanche records or areas with inconsistent avalanche observations (Butler and
57 Malanson, 1985a; Germain et al., 2009; Reardon et al., 2008; Šilhán and Tichavský, 2017; Voiculescu et al.,
58 2016), and many studies used these techniques to examine avalanches across space and time (Table A1).

59 **1.2 Framework and objectives**

60 Tree-ring avalanche research is resource and time intensive. Like other scientific fields, it is not feasible to
61 completely sample the variable of interest with infinite detail due to logistical and financial constraints
62 (Skøien and Blöschl, 2006). Thus, a strategic spatial sampling method is necessary. Here, we strategically
63 sampled 12 avalanche paths in four distinct sub-regions of the U.S. northern Rocky Mountains of northwest
64 Montana to examine spatial differences at a regional scale. The sampling strategy is based on the concept of
65 scale triplet, which defines the spacing, extent, and support of our sampling scheme (Blöschl and Sivapalan,

66 1995). Incorporating the scale triplet concept helps us understand the nature of the problem, the scale at which
67 measurements should be made, and how we can estimate the measurements across space. Often, the scale at
68 which samples are collected differs from the scale necessary for predictive purposes (Blöschl, 1999). For
69 example, if we are interested in avalanche frequency relationships with regional climate patterns but tree-
70 ring samples are collected at an avalanche path scale, then a network of sampled paths need to be spaced and
71 aggregated across the core of the climatically similar region. In our study, the extent is the entire region and
72 sub-regions, the spacing is the distance between avalanche paths and sub-regions, and the support is the size
73 of the area being sampled. In addition, the process scale is the natural variability of avalanche frequency, the
74 measurement scale is the tree-ring proxies used to represent avalanche occurrence on an annual temporal
75 scale, and the model scale relates to aggregating all of the sample areas to derive a regional avalanche
76 chronology.

77 We adopt Martin and Germain's (2016) definition that large magnitude avalanches are events characterized
78 by low and variable frequency with a high capacity for destruction. This generally translates to a size 3 or
79 greater on the destructive classification scale - i.e. ability to bury or destroy a car, damage a truck, destroy a
80 wood frame house, or break a few trees (Greene et al., 2016).

81 Understanding the spatiotemporal behavior of large magnitude avalanches on the regional scale will improve
82 avalanche forecasting efforts, especially for operations involving avalanche terrain that impacts
83 transportation corridors. Here, we aim to answer three specific questions:

84 1) What is the regional, sub-regional, and path specific frequency of large magnitude avalanches in the U.S.
85 northern Rocky Mountains of northwest Montana?

86 2) How does the spatial extent of the study region affect the resultant avalanche chronology?

87 3) What is the probability of detecting regional avalanche activity by sampling different avalanche paths?

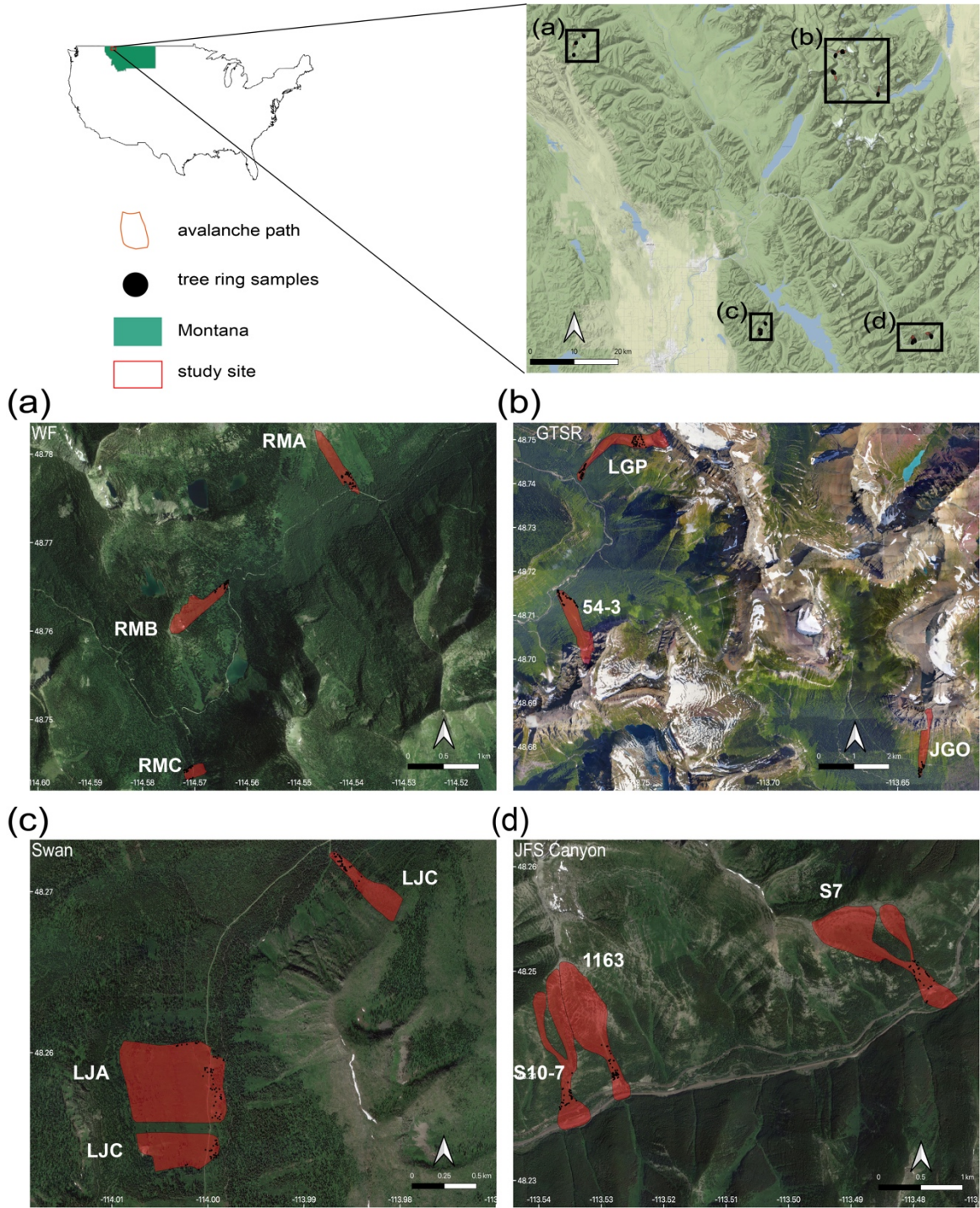
88 To our knowledge, this is the first study to look at how various spatial scales compare when reconstructing a
89 regional avalanche chronology from dendrochronological data on a large dataset ($N > 600$ samples). Further,
90 we believe this is the first study that utilizes a regional dendrochronological record to derive return periods
91 over a large ($> 3500 \text{ km}^2$) spatial extent. Our hypothesis is that aggregating the paths into sub-region and
92 then again into a full region allows us to minimize the limitation of tree-ring avalanche chronologies
93 underestimating avalanche years at these scales.

94 **2. Methodology**

95 **2.1 Study Site**

96 Our study site consists of 12 avalanche paths in the Rocky Mountains of northwest Montana, USA (Figure 1
97 and Table 1). We sampled sets of three avalanche paths in four distinct sub-regions within three mountain
98 ranges: the Whitefish Range (WF, Red Meadow Creek) and Swan Range (Swan, Lost Johnny Creek) on the
99 Flathead National Forest, and two sub-regions within the Lewis Range in Glacier National Park (GNP),
100 Montana. The sites in GNP are along two major transportation corridors through the park: the Going-to-the-

101 Sun Road (GTSR) and U.S. Highway 2 in John F. Stevens (JFS) Canyon. These two areas were utilized for
102 previous dendrochronological avalanche research (Butler and Malanson, 1985a; Butler and Malanson,
103 1985b; Butler and Sawyer, 2008; Reardon et al., 2008). A robust regional avalanche chronology
104 reconstruction will help place the previous work in context of the wider region. The other two sites, WF and
105 Swan, are popular backcountry recreation areas with access via snowmachine in the winter along a U.S.
106 Forest Service road. The avalanche paths in each sub-region encompass a range of spatial extents from
107 adjacent (i.e. < 30 m apart) to ~10 km apart. Overall, this study region provides an ideal natural setting for
108 studying avalanches due to its geography, inclusion of transportation and recreation corridors potentially
109 impacted by avalanches, relative accessibility, and no artificial avalanche hazard mitigation.



110

111 **Figure 1: Study site.** The red rectangle in the state of Montana designates the general area of the four sampling
 112 sites. The sites are (a) Red Meadow, Whitefish Range (WF), (b) Going-to-the-Sun Road (GTSR), central GNP, (c)
 113 Lost Johnny Creek, northern Swan Range (Swan), and (d) John F. Stevens Canyon (JFS), southern GNP. Black
 114 dots represent sample locations. Abbreviated names of each path are in white text adjacent to red polygons (paths).
 115 Satellite and map imagery: © Google (n.d.). Maps produced using ggmap in R (Korpela et al., 2019).

116

117 **Table 1: Topographic characteristics of all avalanche paths. * denotes two major starting zones for one runout in**
 118 **Shed 10-7 and Shed 7 paths.**

Path	Trees (n)	Full Path Elev. (mean) (m)	Full Path Elev. (range) (m)	Starting Zone Elev. (mean) (m)	Full Path Slope (mean) (°)	Starting Zone Slope (mean) (°)	Median Aspect (°)	Area (km ²)	Length (m)	Vertical (m)	Years of previous fire or logging
WF-Red Meadow A (RMA)	41	1651	1462 - 1957	1774	26	32	155	0.32	1004.97	495.20	1952
WF-Red Meadow B (RMB)	40	1870	1643 - 2164	1965	31	37	53	0.13	1041.98	521.27	1967
WF-Red Meadow C (RMC)	42	1650	1582 - 1742	1692	28	33	257	0.08	326.14	160.46	1962
GTSR - 54-3	56	1501	1080 - 2149	1708	31	40	327	0.44	2063.61	1068.49	NA
GTSR-Little Granite (LGP)	109	1770	1109 - 2314	2170	24	34	250	0.78	2940.29	1205.07	NA
GTSR-Jackson Glacier Overlook (JGO)	41	1863	1500 - 2660	2090	32	42	180	0.70	1793.13	1159.84	NA
Swan-Lost Johnny A (LJA)	53	1619	1441 - 1896	1731	29	38	77	0.41	811.50	455.27	1971-72
Swan-Lost Johnny B (LJB)	26	1633	1478 - 1879	1721	32	39	76	0.57	617.52	401.80	1971-72
Swan-Lost Johnny C (LJC)	42	1550	1344 - 1750	1670	34	36	326	0.39	667.88	405.66	1957, 2003
JFS-Shed 10-7 (S10.7)*	109	1644	1233 - 2193	1910 - 1964	31	35 - 39	176	0.13	1745.66	959.74	1910
JFS-Shed 7 (S7)*	46	1712	1310 - 2078	1935 - 1837	29	34 - 36	152	0.57	1686.96	768.01	1910
JFS-1163	50	1718	1250 - 2217	1861	38	42	158	0.17	1636.52	966.82	1910
All Paths	655	1690	1080 - 2660	1869	-0.17	0.14	31	37	Spatial footprint = 3500 km ²		

120 Northwest Montana's avalanche climate is classified as both a coastal transition and intermountain avalanche
121 climate (Mock and Birkeland, 2000), but it can exhibit characteristics of both continental or coastal climates.
122 The elevation of avalanche paths within the study sites range from approximately 1100 m to 2700 m and the
123 starting zones of these paths are distributed among all aspects (Table 1).

124 We eliminated or minimized influence from exogenous disturbance factors such as logging and wildfire by
125 referencing wildfire maps extending back to the mid-20th century. We selected sites undisturbed by wildfire
126 since this time except for Lost Johnny Creek, which was purposeful as this area burned most recently in 2003.
127 We also minimized the influence of logging by selecting sites not previously logged. Using historical logging
128 parcel spatial data, we determined logging in some sites was limited to very small parcels adjacent to the
129 farthest extent of the runout zones.

130 The historical observational record in this area is limited. In this study region, the Flathead Avalanche Center
131 (FAC), a regional U.S. Forest Service backcountry avalanche center, records all avalanches observed and
132 reported to the center. However, not all avalanches are observed or reported given the approximately 3500
133 km² advisory area. The Burlington-Northern Santa Fe Railway (BNSF) Avalanche Safety Program records
134 most avalanches observed in John F. Stevens Canyon in southern Glacier National Park, where there is 16
135 km of rail line with over 40 avalanche paths. However, systematic operational observations only began in
136 2005. Observations prior to this time are inconsistent, though large magnitude avalanches were mostly
137 recorded. Reardon et al. (2008) developed as complete a record as possible from the Department of
138 Transportation and railroad company records, National Park Service ranger logs, and popular media archives.
139 In this sub-region, avalanche mitigation is conducted on an infrequent and inconsistent basis in emergency
140 situations, which is typically only once a year, if at all. Thus, the record approximates a natural avalanche
141 record. We compared the reconstructed avalanche chronology of the JFS sub-region to the historical record
142 of large magnitude years for qualitative purposes. A quantitative comparison would not be reflective of the
143 true reliability of tree-ring methods because of the incomplete historical record.

144 **2.2 Sample Collection and Processing**

145 Our sampling strategy targeted an even number of samples collected from both lateral trimlines at varying
146 elevations and trees located in the main lower track and runout zone of the selected avalanche paths. This
147 adequately captured trees that were destroyed and transported, as well as those that remained in place. The
148 definition of large magnitude avalanche in this study refers to avalanches of approximately size D3 or greater
149 (Greene et al., 2016) and may not run the full length of the avalanche path. We sampled spatial extents within
150 each avalanche path representative of runout extents \geq size D3 avalanches. We also used recent (within the
151 previous 10 years) observed large magnitude avalanche activity in these paths to constrain our sampling.

152 Sample size for avalanche reconstruction using tree-ring data requires careful consideration. Butler and
153 Sawyer (2008) suggested that a few damaged trees may be sufficient for avalanche chronologies, but larger
154 target sample sizes increase the probability of detecting avalanche events (Corona et al., 2012). Germain et
155 al. (2010) examined cumulative distribution functions of avalanche chronologies and reported only slight

156 increases in the probability of extending chronologies with sample size greater than 40. This also depends on
157 the available length of record within a given avalanche path. Thus, given the large spatial footprint (~3500
158 km²) of this study and feasibility of such a large sample size, we sampled between 26-109 samples per
159 avalanche path resulting in 655 trees (Table 2). Eight trees were unsuitable for analysis leaving us with 673
160 total samples from 647 trees. Of the 673 total samples, we collected 614 cross sections and 59 cores. Shed
161 10.7 (S10.7) path was the focus of previous work (Reardon et al., 2008), and the dendrochronological record
162 extends up to 2005 (n=109 trees). Little Granite Path (LGP) was collected in the summer of 2009 (n=109
163 trees). We sampled the remaining 10 paths (437 of the 655 total trees) in the summer of 2017.

164 We collected three types of samples: (1) cross sections from dead trees, (2) cross sections from the dead
165 leaders of avalanche-damaged but still living trees, and (3) cores from living trees. We used predominantly
166 cross-sections in this study for a more robust analysis as events can potentially be missed or incorrectly
167 identified in cores. We emphasized the selection of trees with obvious external scars and considered location,
168 size, and potential age of tree samples. A limitation of all avalanche dendrochronology studies is that large
169 magnitude events cause extensive damage and high tree mortality, thereby reducing subsequent potential
170 tree-ring records.

171 We sampled stem cross-sections at the location of an external scar or just above the root buttress from downed
172 or standing and dead trees, and from stems of trees topped by avalanche damage. We extracted tree-ring core
173 samples from live trees with obvious scarring or flagging along the avalanche path margins and runout zone
174 using a 5 mm diameter increment borer. We collected a minimum of two and up to four core samples per tree
175 (two in the uphill-downhill direction and two perpendicular to the slope). We photographed each sample at
176 each location and recorded species, Global Positioning System (GPS) coordinates (accuracy 1-3 m), amount
177 of scarring on the cambium of the tree, relative location of the tree in the path, and upslope direction (Peitzsch
178 et al., 2019). We also recorded location characteristics that identified the tree to be in-place vs. transported
179 from its original growth position (i.e. presence or absence of roots attached to the ground or the distance from
180 an obvious excavated area where the tree was uprooted).

181 To prevent radial cracking and further rot, we dried and stabilized the cross sections with a canvas backing.
182 We sanded samples using a progressively finer grit of sandpaper to expose the anatomy of each growth ring,
183 and used the visual skeleton plot method to account for missing and false-rings and for accurate calendar
184 year dating (Stokes and Smiley, 1996). We assessed cross-dating calendar-year accuracy of each sample and
185 statistically verified dating against measured samples taken from trees within the gallery forest outside the
186 avalanche path, and from preexisting regional chronologies (Table A2) (ITRDB, 2018) using the dating
187 quality control software COFECHA (Grissino-Mayer, 2001; Holmes, 1983). For further details on cross-
188 dating methods and accuracy calculation for this dataset see Peitzsch et al. (2019).

189 **2.3 Avalanche Event Identification**

190 We analyzed samples for signs of traumatic impact events (hereafter “responses”) likely caused by snow
191 avalanches. We adapted a classification system from previous dendrogeomorphological studies to

192 qualitatively rank the trauma severity and tree growth response from avalanche impacts using numerical
 193 scores ranked 1 through 5 (Reardon et al., 2008). This classification scheme identified more prominent
 194 avalanche damage responses with higher quality scores, and allowed us to remain consistent with previous
 195 work (Corona et al., 2012; Favillier et al., 2018) (Table 2). To compare our ability to capture
 196 avalanche/trauma events using cores versus those captured using cross-sections, we sampled a subset (n=40)
 197 of the cross-sections by analyzing four 5 mm wide rectangles to mimic a core sample from an increment
 198 borer. The four subsamples on each cross section were made perpendicular to one another (i.e. 90 degrees)
 199 based on the first sample taken from the uphill direction of each stem to replicate common field sampling
 200 methods. We then summarized results from the four subsamples for each tree by taking the highest response
 201 score for each growth year. Finally, we compared the number, quality response category, and calendar year
 202 of the avalanche/trauma events derived from the core subsamples to those identified from the full cross
 203 sections.

204

205 **Table 2: Avalanche impact trauma classification ratings, where C1 represents the strongest and easily detectable**
 206 **trauma and C5 represents subtle and difficult-to-detect trauma.**

Classification	Description
C ₁	<ul style="list-style-type: none"> • Clear impact scar associated with well-defined reaction wood, growth suppression or major traumatic resin duct development. • Or, the strong presence of some combination of these major anatomical markers of trauma and growth response recorded in multiple years of growth and occurring at a year that multiple samples from other trees at the site record similar trauma and scarring. • C₁ events are also assigned to the death date of trees killed by observed avalanche mortality at the collection site; the presence of earlywood indicates an early spring, or late avalanche season, event killed the tree.
C ₂	<ul style="list-style-type: none"> • Scar or small scar recorded in the first ten years of tree growth without associated reaction wood, growth suppression or traumatic resin ducts. • Or, obvious reaction wood, growth suppression or significant presence of traumatic resin ducts that occur abruptly after normal growth that lasts for 3 or more years.
C ₃	<ul style="list-style-type: none"> • The presence of reaction wood, growth suppression, or traumatic resin ducts recorded in less than 3 successive growth years.
C ₄	<ul style="list-style-type: none"> • Poorly defined reaction wood, growth suppression or minimal presence of traumatic resin ducts lasting 1-2 years. • Or, a C₃ class event occurring in the first 10 years of tree growth where the cause of damage could result from various biological and environmental conditions.
C ₅	<ul style="list-style-type: none"> • Very poorly defined reaction wood, growth suppression, or minimal presence of traumatic resin ducts isolated in one growth year. • Or, a C₄ class event occurring in the first 10 years of tree growth where the cause of damage could result from various biological and environmental conditions.

207

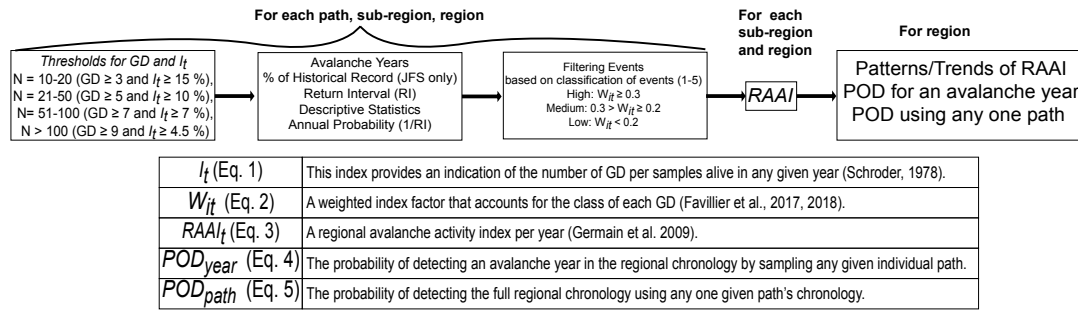
208 2.4 Chronology and Return Period Calculation

209 To generate avalanche event chronologies and estimate return periods for each path and for the entire study
 210 site, we utilized *R* statistical software and the package *slideRun*, an extension of the *burnR* library for forest
 211 fire history data (Malevich et al., 2018). We calculated the age of each tree sampled and the number of
 212 responses per year in each avalanche path and computed descriptive statistics for the entire dataset. Estimates
 213 of avalanche path return intervals should be viewed as maximum return interval values due to the successive
 214 loss of samples and decreasing sample number back through time.

215 We used a multi-step process to reconstruct avalanche chronologies on three different spatial scales:
 216 individual paths, four sub-regions, and the entire region. We also calculated a regional avalanche activity
 217 index (RAAI) (Figure 2). The process involved first calculating the ratio of trees exhibiting growth
 218 disturbance (GD) over the number of samples alive at year t to provide the index I_t (Shroder, 1978):

$$I_t = \left(\frac{\sum_{i=1}^n (R_t)}{\sum_{i=1}^n (A_t)} \right) \times 100 \quad (1)$$

219 where R is the number of trees recording a GD at year t with A_t representing the number of trees alive in our
 220 samples at year t .



221

222 **Figure 2: General workflow of analytical methods to reconstruct regional avalanche chronology, regional**
 223 **avalanche activity index, and the probability of detection. N=sample size. GD=growth disturbances. I_t = Index of**
 224 **ratio of responses to trees alive. RI=return interval. W_{it} =weighted index as per Favillier (2017, 2018).**
 225 **RAAI=regional avalanche activity index as per Germain et al. (2009). POD = probability of detection. See Eqs. 1-**
 226 **5 for details.**

227 We then used double thresholds to estimate the minimum absolute number of GD and a minimum percentage
 228 of samples exhibiting GD per year (I_t) based on sample size (N) following thresholds established by Corona
 229 et al. (2012) and Favillier et al. (2018): $N = 10-20$ ($GD \geq 3$ and $I_t \geq 15\%$), $N = 21-50$ ($GD \geq 5$ and $I_t \geq 10$
 230 $\%$), $N = 51-100$ ($GD \geq 7$ and $I_t \geq 7\%$), and $N > 100$ ($GD \geq 9$ and $I_t \geq 4.5\%$).

231 We then used the chronologies derived from this process to calculate a weighted index factor (W_{it}). We used
 232 this established threshold approach since it has been broadly employed in the literature and allows
 233 comparability of our avalanche chronology to results reported in other studies. We adapted previous
 234 equations of a weighted response index (Kogelnig-Mayer et al., 2011) to our 5-scale ranking quality
 235 classification to derive the W_{it} :

$$W_{it} = \frac{\left(\left(\sum_{i=1}^n T_{C_1} * 7 \right) + \left(\sum_{i=1}^n T_{C_2} * 5 \right) + \left(\sum_{i=1}^n T_{C_3} * 3 \right) + \left(\sum_{i=1}^n T_{C_4, C_5} \right) \right)}{\sum_{i=1}^n A_t} \quad (2)$$

236 where the sum of trees with scars or injuries ($C_1 - C_5$) were multiplied by a factor of 7, 5, 3, 1 and 1
 237 respectively (Kogelnig-Mayer et al., 2011).

238 Next, we classified W_{it} into high, medium, and low confidence events using the thresholds detailed in Favillier
 239 et al. (2018), where High: $W_{it} \geq 0.3$, Medium: $0.3 > W_{it} \geq 0.2$, Low: $W_{it} < 0.2$. This provided another step
 240 discriminating the avalanche response from noise. We included all events with medium to high confidence
 241 in the next analysis. We then estimated the number of avalanche years, descriptive statistics for return
 242 intervals (RI), and the annual probability (1/RI) for each path, sub-region, and region. We use these RI values
 243 determined after filtering events throughout the study. We then compared return intervals for all individual
 244 paths and sub-regions using analysis of variance (ANOVA) and Tukey's Honest Significant Difference
 245 (HSD) (Ott and Longnecker, 2016). In the final step of RI analysis, we subset the period of record for each
 246 path from 1967-2017 to compare RI from this condensed time series to the full period of record for each path.
 247 Next, we compared the number of avalanche years and return periods identified in the full regional
 248 chronology to subsets of the region to determine the number of paths required to replicate a full 12-path
 249 regional chronology. We assessed the full chronology against a subsampling of 11 total paths by sequentially
 250 removing the three paths with the greatest sample size. We then randomly sampled two paths from each sub-
 251 region for a total subsample of eight paths, followed by generating a subsample of four paths by choosing
 252 the path in each sub-region with the greatest sample size. Finally, we selected a random sample of one path
 253 from each sub-region to compare against a total of four single path subsamples.

254 **2.5 Regional Avalanche Activity Index and Probability of Detection**

255 Next, we used the I_t statistic from each path to calculate a regional avalanche activity index (RAAI) for the
 256 sub-regions and overall region (Germain et al., 2009). The RAAI for each year across the sub-regions and
 257 region provides a more comprehensive assessment of avalanche activity within the spatial extent. For each
 258 year t , we calculated RAAI:

$$RAAI_t = \left(\sum_{i=1}^n I_t \right) / \left(\sum_{i=1}^n P_t \right) \quad (3)$$

259 where I is the index factor as per Eq. (1) for a given avalanche path for year t and P is the number of paths
 260 that could potentially record an avalanche for year t . For the calculation of the overall RAAI, we required
 261 each path to retain a minimum sample size of ≥ 10 trees with a minimum number of three paths for year t ,
 262 and a minimum of one path from each sub-region. We performed a sensitivity test to establish the minimum
 263 number of paths necessary to calculate an RAAI value for any given year.

264 We also calculated the probability of detecting an avalanche year identified in the regional chronology as if
 265 any given individual path was sampled. The probability of detection for a given year (POD_{year}) is defined as:

$$POD_{year} = \frac{a}{a + b} \quad (4)$$

266 where a is the number of individual avalanche paths that identify any given avalanche year in the regional
 267 chronology and b is the total number of avalanche paths ($n=12$). We calculated POD_{year} for every year in the
 268 regional avalanche chronology. We then compared the POD_{year} of individual paths to the number of active
 269 avalanche paths as defined in Eq. (3).

270 We also calculated the probability of detection for each path for the period of record (POD_{path}):

$$POD_{path} = \frac{c}{c + d} \quad (5)$$

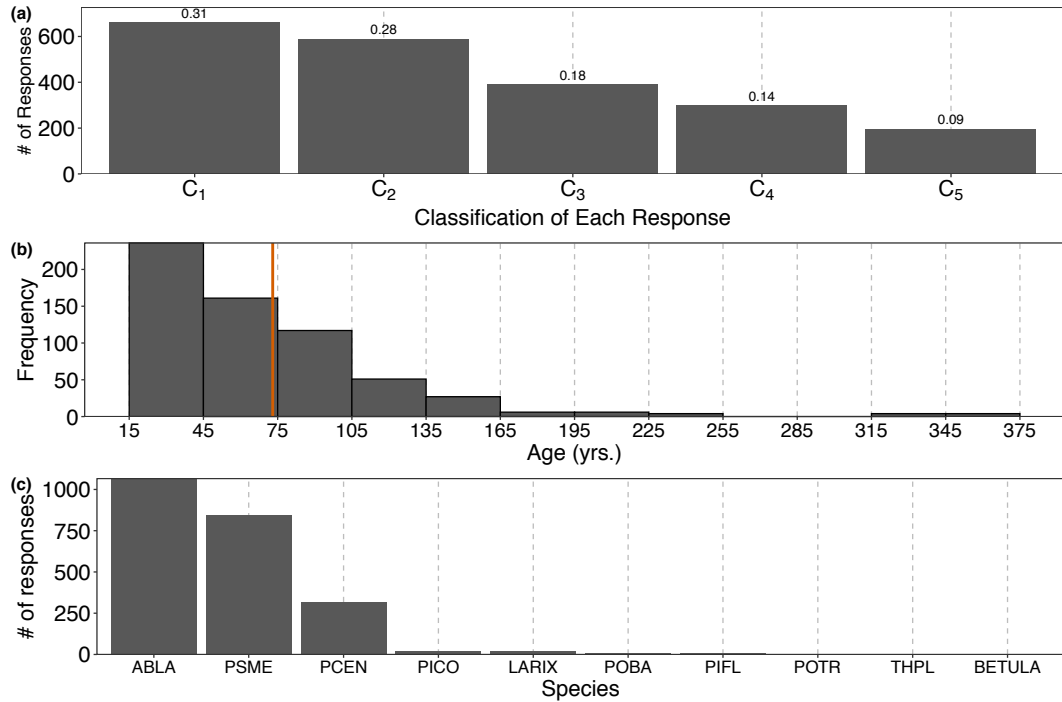
271 where c is the number of years identified in any given path that is included in the regional chronology and d
 272 is the number of years in the regional chronology that are not identified in the chronology for the given path.

273 2.6 Geomorphological characteristics

274 Using a 10 m digital elevation model (DEM), we calculated a number of geomorphological characteristics
 275 for each path, including mean elevation (m, full path and starting zone), elevation range (m), eastness
 276 ($\sin(\text{aspect})$) and northness ($\cos(\text{aspect})$) (radians), slope (degrees, full path and starting zone), curvature
 277 (index (0-1), profile and planform), roughness (index, full path and starting zone), perimeter (km²), area
 278 (km²), length (m), and vertical distance from starting zone to runout zone (m). We also calculated the mean
 279 of these characteristics for all paths in the region. The geomorphological characteristics allowed for a
 280 determination of the representativeness of the region as a whole (i.e. are the paths similar across the region?)
 281 as well as a comparison of the return interval for each path relative to these characteristics. Finally, we
 282 estimated the potential relationship between path length, starting zone slope angle, the number of avalanche
 283 years, and median return interval for each individual path using the Pearson correlation coefficient.

284 3. Results

285 We collected a total of 673 samples from 647 suitable avalanche impacted or killed trees (trees: $n = 531$ dead;
 286 $n = 116$ living) in the full 12-path regional avalanche collection. Of those 673 samples, 614 were cross
 287 sections (91%) and 59 were cores (9%). Within these samples we identified 2134 GD, of which 1279 were
 288 classified as C₁ and C₂ (60%) (Figure 3(a)). Scars were the dominant input type in GDs classified as C₁, and
 289 reaction wood comprised the majority of GDs classified as C₂, C₃, and C₄ (Table A3) The oldest individual
 290 tree sampled was 367 years, and the mean age of all samples was 73 years (Figure 3(c)). The period of record
 291 of sampled trees extended from 1636 to 2017 C.E. The most common species in our dataset was *Abies*
 292 *lasiocarpa* (ABLA, sub-alpine fir) (46%) followed by *Pseudotsuga menziesii* (PSME, Douglas-fir) (37%)
 293 and *Picea engelmannii* (PIEN, Engelmann spruce) (14%) (Figure 3(d)). The oldest GD response dates to year
 294 1655. In the entire dataset, the five years with the greatest number of raw GD responses were 2002 (165
 295 responses), 2014 (151 responses), 1990 (93 responses), 1993 (90 responses), and 1982 (75 responses).

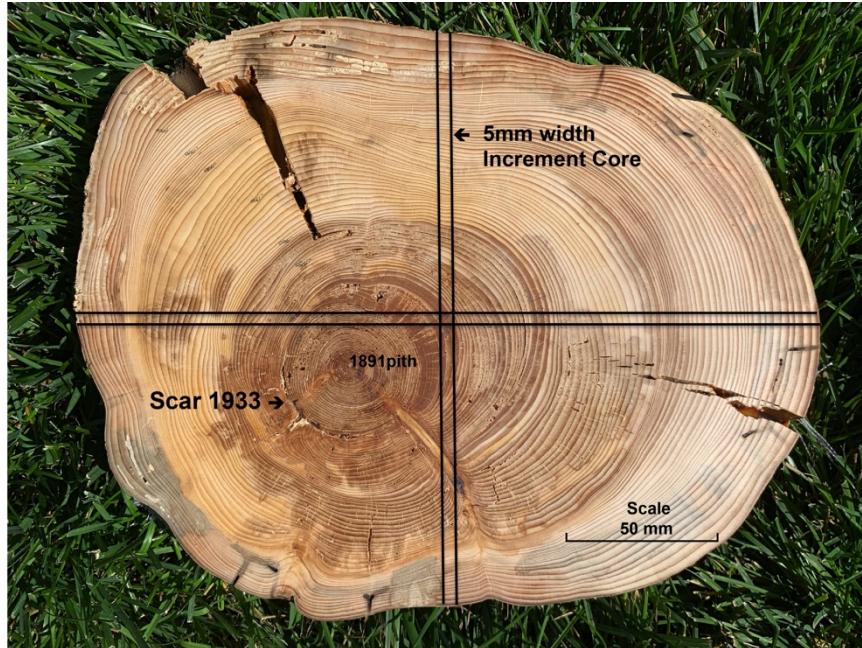


296

297 **Figure 3: Histograms of (a) number of classification of responses (number above bar represents proportion), (b)**
 298 **sample age (red line represents mean age), and (c) collected species. For species: ABLA=*Abies Lasiocarpa*, PCEN**
 299 **= *Picea engelmannii*, PSME = *Pseudotsuga menziesii*, THPL = *Thuja plicata*, PICO = *Pinus contorta*, POTR =**
 300 ***Populus tremuloides*, LARIX = *Larix* Mill., BETULA = *Betula* L., POBA = *Populus balsamifera*.**

301 3.1 Avalanche Event Detection: Cores versus Cross-Sections

302 The avalanche response subset analysis that compared results as if samples were from cores versus full cross
 303 sections showed that core samples alone would have missed numerous avalanche events and generated a
 304 greater proportion of low-quality growth disturbance classifications (Figure 4). For the subset of 40 samples
 305 analyzed as cores we identified only 124 of 191 (65%) total GD. Of the 67 GDs that we would have missed
 306 just by using cores, 24 were classified as C₁ quality events, 24 were C₂, 14 were C₃, 3 were C₄, and 2 were
 307 C₅ (Table A4).

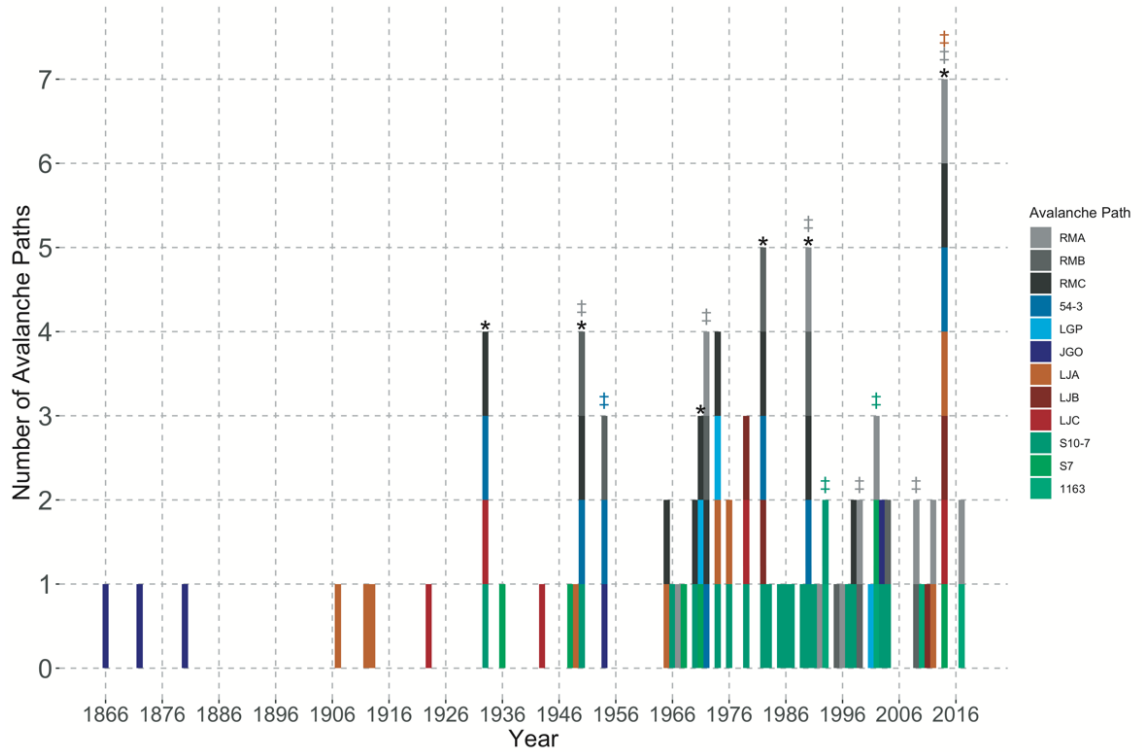


308

309 **Figure 4:** Example of cross section sample where 4 cores taken on uphill, downhill, and perpendicular (2) would
 310 have missed at least one scar (1933) and potentially the pith of the tree. The black lines indicate the potential cores
 311 using a 5 mm width increment borer. Note scale on lower right of sample.

312 3.2 Individual Path Chronologies

313 There were 49 avalanche events identified from GD responses across all 12 individual paths in the study
 314 region. The avalanche years most common throughout all of the individual path chronologies were: 2014 (7
 315 paths); 1982 and 1990 (5 paths); and 1933, 1950, 1972, and 1974 (4 paths) (Figure 5 and Table 3). We
 316 identified the year with the greatest number of individual GD responses (2002) in 3 paths - two from JFS
 317 sub-region and one in the WF sub-region. There was no clear pattern of similarly identified years from paths
 318 physically closer in proximity to each other. However, paths within the WF sub-region produced the most
 319 similar number of large magnitude avalanche years. When we applied the W_{it} process step, the number of
 320 identified avalanche years did not change for any individual avalanche path compared to application of the
 321 double threshold method alone. This highlights the number of responses classified as C_1 and C_2 (high quality)
 322 in our dataset.



323

324 **Figure 5: Number of individual avalanche paths in which an avalanche event occurred in any given year.**
 325 **Avalanche years with † (gray=WF, dark blue = GTSR, orange = Swan, green= JFS) indicate years identified in at**
 326 **least two avalanche paths in the sub-region. * represents avalanche years in common in at least 1 path from at**
 327 **least three of the four sub-regions.**

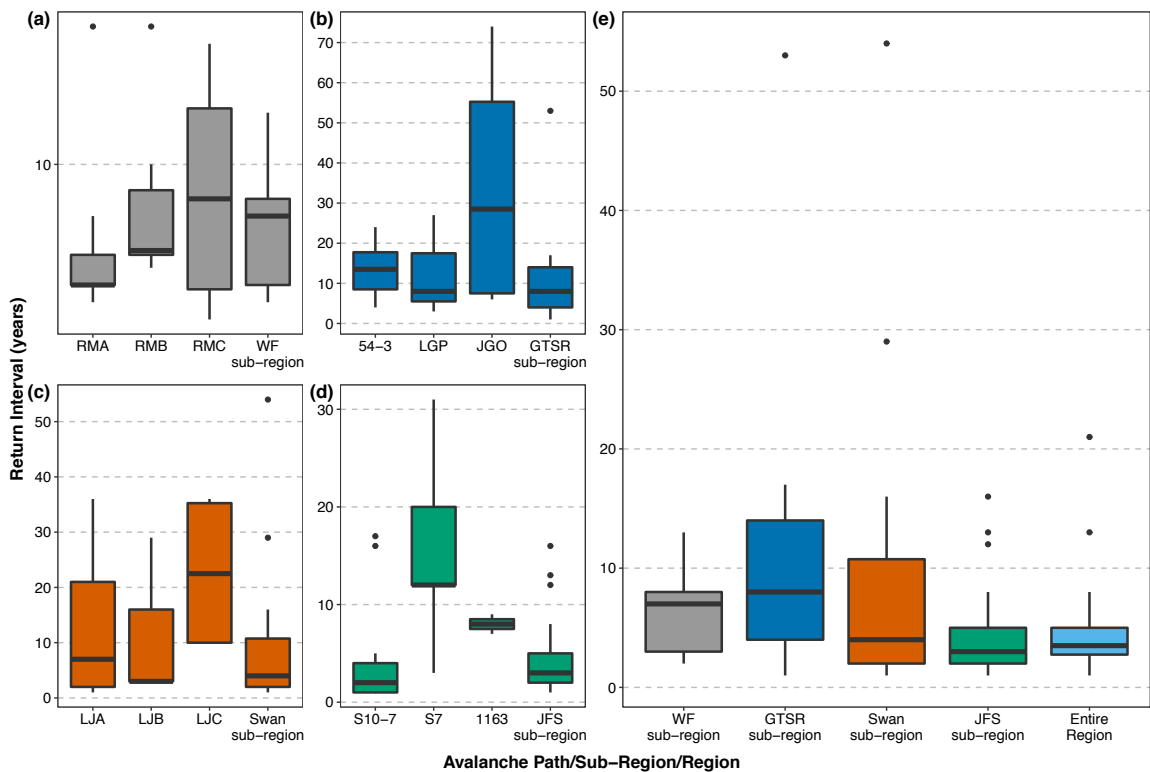
328

329 **Table 3: Avalanche chronologies and return interval (RI) statistics of all 12 avalanche paths in the region.**
 330 **Avalanche years in bold indicate years identified in at least two avalanche paths in the sub-region. Underlined**
 331 **avalanche years indicate years in common in at least 1 path from at least three of the four sub-regions. 1/RI refers**
 332 **to the probability of an avalanche occurring in that avalanche path in any given year. σ refers to the standard**
 333 **deviation of the RI. The period of record (POR) for each path represents earliest inner year to the most recent**
 334 **outer year of all raw samples in the path. The RI was calculated on the return interval of avalanche years.**

Sub-region	WF			GTSR			Swan			JFS		
Path	RMA	RMB	RMC	54-3	LGP	JGO	LJA	LJB	LJC	Shed 10-7	Shed 7	1163
Aval Years	1967 1972 <u>1990</u> 1992 1996 1999 2002 2009 2012 <u>2014</u> 2017	1950 1954 <u>1954</u> 1972 <u>1982</u> 1990 1995 1999 2004 2009 2017	<u>1933</u> 1950 1965 1970 <u>1971</u> 1972 <u>1974</u> 1982 <u>1990</u> 1998 2014	<u>1933</u> <u>1950</u> 1954 1972 <u>1974</u> 2001 <u>1982</u> <u>1990</u> <u>2014</u>	<u>1971</u> <u>1974</u> 2001 2009	1866 1872 1880 1954 2003	1907 1912 1913 1949 1965 <u>1974</u> 1976 2012 2014	1979 <u>1982</u> 2011 2014	1923 <u>1933</u> 1943 1979 2014	<u>1933</u> <u>1950</u> 1966 1970 <u>1974</u> 1976 1979 <u>1982</u> 1983 <u>1985</u> 1986 1987 1989 <u>1990</u> 1991 1993 1997 1998 2003 2004	1936 1948 1968 1971 2002 <u>2014</u>	1993 2002 2010 2017
# of aval. years	11	9	11	7	4	5	9	4	5	20	6	4
POR (raw samples)	1922-2017	1845-2017	1783-2016	1777-2017	1836-2009	1784-2017	1636-2017	1808-2017	1657-2017	1910-2004	1864-2017	1929-2017
RI median	3	5	8	14	8	28.5	7	3	22.5	2	12	8
RI - mean	5	7.38	8.1	13.5	12.67	34.25	13.38	11.67	22.75	3.74	15.6	8
RI - min.	2	4	1	4	3	6	1	3	10	1	3	7
RI - max.	18	18	17	24	27	74	36	29	36	17	31	9
1/RI	0.33	0.20	0.13	0.07	0.13	0.13	0.14	0.33	0.04	0.50	0.08	0.13
σ	4.81	4.78	6.12	7.42	12.66	33.09	14.79	15.01	14.73	4.68	10.50	1.00

335
 336 Across all individual paths, the median estimated return interval was 8 years with a range of 2 to 28.5 (Figure
 337 6). Hereafter return intervals indicate median return intervals unless specified. JGO, located in the GTSR
 338 sub-region, exhibited the greatest spread in estimated return intervals followed by LJB. The avalanche paths
 339 within the WF sub-region had the most similar return intervals of any of the sub-regions. The return interval

340 for JGO differed significantly from several other paths: RMA, RMB, RMC, and Shed 10-7 ($p \leq 0.01$).
 341 However, when we relax a strict cutoff of $p = 0.05$, the return interval from JGO also differed from 1163 (p
 342 $=0.07$) and LJA ($p = 0.08$). Similarly, the return interval for Shed 10-7 differs from LJC ($p = 0.07$). In
 343 assessing the potential geomorphic controls on return interval, path length was the only significantly
 344 correlated characteristic ($r = 0.65$, $p = 0.02$, Figure A1).
 345 We subset the period of record for each path from 1967-2017 and compared RI values to the full record. In
 346 this subset, nine paths exhibit no change in RI values when compared to the full record. In one path, 54-3, RI
 347 values decreased from 14 to 10 years. We observed larger changes in the other two paths; JGO path where
 348 only one avalanche year was recorded (down from 5 years) and the median RI in LJC changed from 22.5
 349 years to 35 years. If we removed 54-3, JGO and LJC for this comparison, the records from the subset period
 350 of record are similar to the complete records for the other paths in the study.



351
 352 **Figure 6: Boxplot of return intervals for individual avalanche paths in each sub-region: (a) WF, (b) GTSR, (c)**
 353 **Swan, and (d) JFS. (e) shows the boxplots of return intervals for the sub-regions and the overall region.**

354 3.2 Sub-region Chronologies

355 When the paths were aggregated into sub-regions (three paths per sub-region) the median return periods for
 356 each sub-region were similar and all less than 10 years (Figure 6(e) and Table 4). The number of avalanche
 357 years for all of the sub-regions ranges from 12-18 with the greatest number of identified years in the JFS sub-
 358 region and the fewest in the WF sub-region. The JFS sub-region has the shortest median return interval
 359 followed by the Swan, WF, and GTSR sub-regions. The number of avalanche years for each aggregated sub-
 360 region is greater than the number of avalanche years for any individual path within each sub-region except

361 for the JFS sub-region where 18 avalanche years were identified but Shed 10-7 totaled 20 avalanche years
 362 (Table 5).

363

364 **Table 4: Avalanche chronologies and return interval (RI) statistics of all four sub-regions. 1/RI refers to the**
 365 **probability of an avalanche occurring in that avalanche path in any given year. σ refers to the standard deviation**
 366 **of the RI.**

367

	WF	GTSR	Swan	JFS	Region
# of aval. years	12	14	13	18	30
RI – median	7	8	4	3	3
RI – mean	6.27	11.35	11.25	4.94	5.21
RI – min.	2	1	1	1	1
RI – max.	13	53	54	16	21
1/RI	0.14	0.13	0.25	0.33	0.33
σ	3.69	13.48	15.70	4.60	9.53

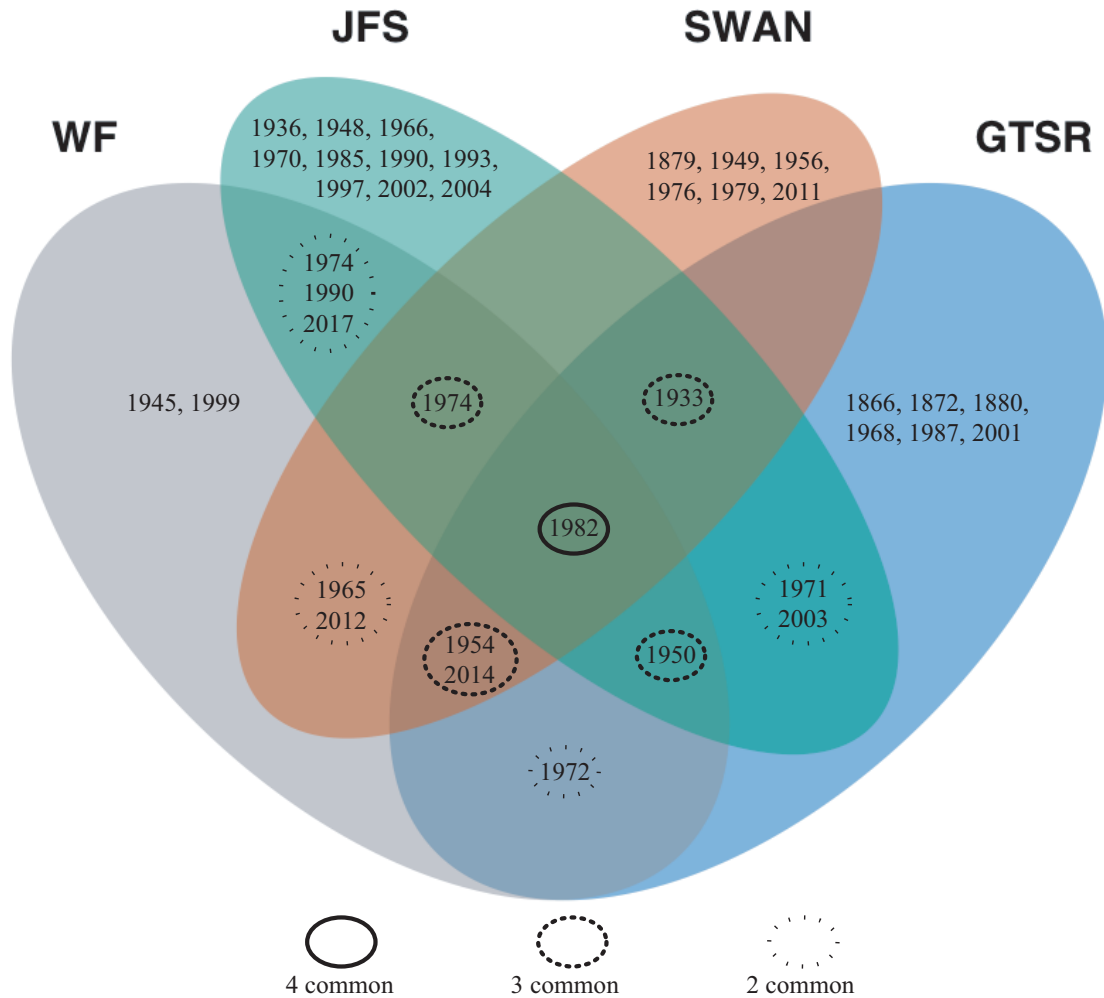
368

369 **Table 5: Number of avalanche events for each subregion, the mean of three individual paths in each region, and**
 370 **the overall aggregated region.**

# of avalanche events		
Sub-region	3 individual paths	Aggregated sub-region
WF	11,9,11	12
GTSR	7,4,5	14
Swan	9,4,5	13
JFS	20,6,4	18
Region		30

371

372 In terms of commonality of years between the sub-regions, 1982 is the only year identified in all of the four
 373 sub-regions (Figure 7). Avalanche years commonly identified in three sub-regions are 1933, 1950, 1954,
 374 1974 and 2014. We identified the JFS sub-region as having the greatest number of years exclusive to that
 375 sub-region (10 years). The WF sub-region shared the greatest number of years with other regions (11 years)
 376 followed by JFS (9 years), GTSR (8 years), and the Swan (7 years). In the only available comparison against
 377 an incomplete and limited historical record, the individual reconstructed avalanche chronologies of paths in
 378 the JFS sub-region captured 10-50% of the recorded large magnitude events over years 1908 to 2017.

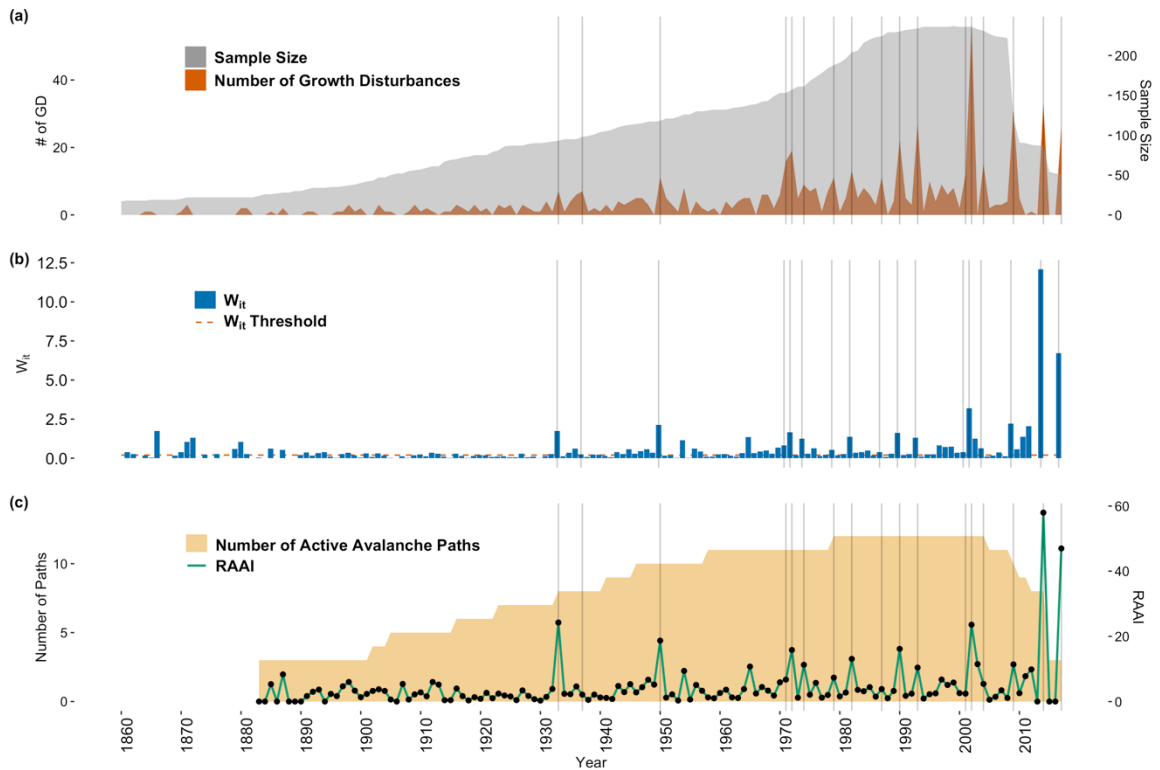


379

380 **Figure 7: Venn diagram of avalanche years common between sub-regions. Overlapping areas of each ellipse**
 381 **indicate years in common with each sub-region.**

382 **3.3 Regional Chronology and RAAI**

383 We identified 30 avalanche years in the overall region and a median return interval of 3 years (Table 5). The
 384 number of samples increases through time to a peak during 2005 and as expected the number of GD also
 385 increases through time (Figure 8(a)). The W_{it} index also increases, particularly from year 2000 onward with
 386 the largest spikes in 2014 and 2017 (Figure 8(b)). The regional assessment of avalanche years identified
 387 fewer years (n=30) than the simple aggregation of all unique avalanche years identified in the individual
 388 paths (n=49) (Table A2).



389

390 **Figure 8: (a) The number of samples (gray shaded area) increases through time, but the number of responses**
 391 **(dark orange shaded area) varies. Note that sample size is on a secondary (right) y-axis. (b) The W_{it} , a weighted**
 392 **index factor that accounts for the class of each growth disturbance, threshold (0.2, red dashed line) provides a**
 393 **means of discriminating between high and low confidence signals in the tree ring record. (c) The Regional**
 394 **Avalanche Activity Index (RAAI) (green line, black points) is a measure of regional avalanche activity based on**
 395 **the I_t , the ratio of trees exhibiting growth disturbance over the number of samples alive at year t , of each path and**
 396 **the number of active avalanche paths (yellow shaded area). Note RAAI is on a secondary (right) y-axis.**

397 When we included all paths but S10.7 (one of two paths with the greatest sample size), we captured 80% of
 398 all avalanche years and added one new year to the chronology (Table 7). When we removed LGP (the other
 399 path with the greatest size of sampled trees), we still captured all of the years in the regional chronology but
 400 introduced four new years into the chronology for a total of 34 years. A random sample of eight (two from
 401 each sub-region) of the 12 avalanche paths captured 83% of the years in the chronology and identified two
 402 new avalanche years. Finally, when using only one path from each sub-region with the largest samples size
 403 (Shed 10-7, 54-3, LJA, and RMA), we captured 73% of the avalanche years identified in the full regional
 404 chronology. When using a random sample of one path from each sub-region (1163, LGP, LJC, RMB), we
 405 captured only 43% of the years included in the regional chronology of all 12 paths. The RAAI is insensitive
 406 (no significant difference, $p > 0.05$) to the number of paths when tested using a minimum number of paths
 407 recording an avalanche in year t . The years with the largest RAAI are 2014 and 2017 followed by 2002, 1950
 408 and 1933 (Figure 8(c)).

409

410 **Table 6: Comparison of the number of avalanche years and return intervals (RI) when including all 12 paths in**
 411 **region to using a combination of fewer paths to define the region. HLC=high level of confidence and**
 412 **MLC=medium level of confidence as per Favillier et al. (2017, 2018). ‘# not in regional’ refers to avalanche years**
 413 **identified in that particular combination of paths but not identified in the regional record.**
 414

Paths	Region (All Paths)	All but S10.7	All but LGP	All but 54-3	S7, 1163, LGP, JGO, RMB, RMC, LJB, LJC	S10.7, 54-3, LJA, RMA	1163, LGP, LJC, RMB
# Paths	12	11	11	11	8	4	4
Sample Size (n)	635	528	526	581	382	253	239
# of Aval Years	30	27	34	31	27	34	17
# matches with regional	NA	24	30	29	25	22	13
# not in regional	NA	1	4	2	2	11	4
% captured in regional	NA	80	100	97	83	73	43
Median RI	3	3	3	3	3	2	3.5
# years removed using only W_{it}= HLC instead of W_{it}=MLC and HLC	10	3	9	7	1	1	1

415

416 The probability of detection for the avalanche years (POD_{year}) identified in the regional chronology ranged
 417 from 8 to 58% when we examined individual paths (Table 7). The year with the highest POD was 2014. The
 418 mean POD for all years was 21%. When we examined avalanche paths that exhibited at least one GD during
 419 avalanche years identified in the regional chronologies (i.e. no thresholds used), the POD is generally greater.

420

421 **Table 7: Probability of Detection (POD_{year}). Avalanche years identified in the regional chronology and associated**
 422 **POD by analyzing individual paths with and without growth disturbances (GD), sample size, and W_{it} thresholds.**

Avalanche Year in Regional Chronology	POD (%) with thresholds	POD (%) without thresholds
1866	8	8
1872	8	8
1880	8	17
1933	33	58
1936	8	25
1945	NA	58
1948	8	33
1950	33	58
1954	25	67
1956	NA	58
1965	17	67
1970	17	50
1971	25	50
1972	33	83
1974	33	75
1976	17	50
1982	42	92
1990	42	83
1993	17	50
1997	8	92
1998	17	50
1999	17	58
2002	25	75
2003	17	33
2004	17	75
2009	17	33
2011	8	33
2012	17	42
2014	58	58
2017	17	25
Mean	21	52

423

424 Finally, the probability of capturing all of the avalanche years identified in the regional chronology by each
 425 individual path ranges from 7% to 40% (Table 8). The greatest POD_{path} value from any given path is S10.7
 426 ($POD = 40\%$) in the JFS sub-region followed by RMC in the Whitefish sub-region ($POD = 37\%$). In general,
 427 the paths within the Whitefish sub-region capture the regional chronology most consistently.

428

429 **Table 8: Probability of Detection of each individual path (POD_{path}) to the regional avalanche chronology.**

Path	POD (%)
RMA	27
RMB	27
RMC	37
54-3	23
LGP	7
JGO	17
LJA	17
LJB	10
LJC	7
Shed 10-7	40
Shed 7	17
1163	10

430 **4. Discussion**

431 The processing and analysis of 673 samples spanning a large spatial extent allowed us to create a robust
 432 regional large magnitude avalanche chronology reconstructed using dendrochronological methods. Cross-
 433 sections provided a more robust and complete GD and avalanche chronology compared to a subsample
 434 generated from cores alone. Due to the reduced information value of working only with cores, Favillier et al.
 435 (2017) included a discriminatory step in their methods to distinguish avalanche signals in the tree-ring record
 436 from exogenous factors, such as abnormal climate signals or response to insect disturbance. By using cross
 437 sections to develop our avalanche chronologies, we were able to view the entire ring growth and potential
 438 disturbance around the circumference of the tree as opposed to the limited view provided by cores. This
 439 allowed us to place GD signals in context to both climate and insect disturbance without the need for this
 440 processing step. We do not discount any studies that use cores for reconstructing avalanche chronologies and
 441 understand there are sampling limitations from environmental and policy perspectives in different regions as
 442 well as financial and processing constraints. However, we are suggesting that if the ability to collect cross
 443 sections exists, then it is advantageous to collect them.

444 We targeted sample collection in the runout zones and along the trim line where large magnitude avalanches
 445 occurred in recent years. At several sites we collected samples at the upper extent of the runout zones (S10.7,
 446 Shed 7, and 1163). Thus, some additional noise in the final chronology for those specific paths could be due
 447 to more frequent small magnitude avalanches. Though the oldest individual trees extended as far back as the
 448 mid-17th century, the application of the double thresholds processing steps restricted individual path
 449 avalanche chronology lengths since the minimum GD threshold requirements were not met. It is difficult to
 450 place confidence in these older recorded events due to the decreasing evidence back in time inherent in
 451 avalanche path tree-ring studies. Therefore, we chose to examine more recent time periods dictated by the
 452 avalanche years identified through the double threshold methods.

453 All of the paths in the study are capable of producing large magnitude avalanches with path lengths greater
 454 than 100 m (typical length for avalanche destructive size 2, D2), and all but RMC have a typical path length

455 of close to or greater than 1000 m (for avalanche destructive size 3, D3) (Greene et al., 2016). As Corona et
456 al. (2012) noted, the avalanche event must be large enough to create an impact on the tree, and size D2 or
457 greater will be evident from the tree-ring record (Reardon et al., 2008). However, the successive damage and
458 removal of trees from events size D2 or greater also impacts the future potential to record subsequent events
459 of similar magnitude. In other words, if a large magnitude avalanche removes a large swath of trees in one
460 year, then there are fewer trees available to record a slightly smaller magnitude avalanche in subsequent
461 years. Therefore, dendrochronology methods inherently underestimate avalanche events by up to 60%
462 (Corona et al., 2012).

463 **4.1 Regional Sampling Strategy**

464 By examining three different spatial scales (individual path, sub-region, and region) we produced a large
465 magnitude avalanche chronology for the region captured in a small subset of the total number of paths across
466 the large region. Accordingly, this sampling strategy may also alleviate the issue of recording large magnitude
467 avalanches within a region in the successive years following a major destructive avalanche event that
468 removed large number of trees within specific paths but not others. Overall, a regional sampling strategy
469 enables us to capture large magnitude avalanche events over a broad spatial extent that is useful for regional
470 avalanche forecasting operations and future climate association analysis. This strategy also allows us to
471 understand large magnitude avalanche activity at scales smaller than the regional scale.

472 **4.2 Chronologies for Individual Paths and Sub-Regions**

473 We applied the W_{it} threshold specifically to weight higher quality responses. The number of identified
474 avalanche years does not change for any individual avalanche path when we applied the W_{it} process. This
475 lack of change suggests that many of the responses in our samples were ranked as high-quality (i.e. C₁-C₂).
476 The high quality of responses can be attributed to the use of cross sections which allowed for a more complete
477 depiction and assessment of the tree-ring signal (Carrara, 1979). Scarring comprised the majority of C₁
478 samples and evidence of scarring in lower quality classification was due to other types of small cambial tissue
479 scars that could not be confidently classified as avalanche damage. The reaction wood in C₁ GDs were
480 associated with obvious avalanche scars in the same year.

481 We developed avalanche chronologies for 12 individual avalanche paths. The path with the greatest number
482 of identified avalanche years, S10.7, contains two major starting zones that are both steeper (35 and 39
483 degrees) than Shed 7, which also contains two separate starting zones. Reardon et al. (2008) collected a
484 substantial number of samples at higher elevations in the S10.7 avalanche path. However, the location data
485 for these samples were not available. Many of those samples were the living stumps that captured smaller
486 annual events. This is likely the root of the difference for S10.7 and the other paths in this study and the
487 reason this path contains the largest numbers of avalanche years in this analysis.

488 The range of return intervals across all paths (2 – 28.5 years) is similar to those reported for 12 avalanche
489 paths across a smaller spatial extent in the Chic Choc Mountains of Quebec, Canada (2 – 22.8) (Germain et

490 al., 2009). Although the authors in that study used a different avalanche response index, their study still
491 suggests considerable variation in avalanche frequency across avalanche paths within a region.

492 The results from examining return intervals during a truncated period from 1967-2017 across all paths
493 illustrate that several of the individual path return interval results should be treated with caution (e.g. JGO,
494 LJC, and 54-3). The difference in minimum and maximum return interval values is a function of a decreasing
495 sample size back in time. The minimum return interval values in many of the paths are concentrated during
496 recent periods. This is a limitation of using dendrochronology to estimate return intervals. Comparing
497 avalanche return intervals across individual paths should also be treated with caution given the variable nature
498 of sample availability across paths. This variability across individual paths further provides reason to evaluate
499 the number of paths necessary to create a regional avalanche chronology from tree rings. Most of the paths
500 have a reasonable record over this truncated period and also highlight the importance of strategic sampling
501 in numerous avalanche paths. While dendrochronology underestimates avalanche activity, we show that
502 sampling enough paths across a region provides a reasonable estimate of avalanche activity at this scale.

503 JGO contains the maximum return interval for any path in the study, and the return intervals are significantly
504 different than numerous other paths. A lack of recording data after one large avalanche event could easily
505 skew this value. To understand if this value is accurate, we would have to sample adjacent tracks to determine
506 if the return intervals are similar or not. An appropriate sample base without large temporal gaps is necessary
507 to fully provide an accurate estimate of return intervals within a single avalanche path. While the sample size
508 is sufficient for this individual path, the results should be treated with caution due to the temporal gaps. In
509 other words, the large return interval values may reflect the irregular preservation of evidence for large
510 avalanches as opposed to an accurate estimate of return intervals. Therefore, we cannot fully explain the large
511 maximum return interval for this path.

512 The return intervals for LJC in the Swan sub-region were the greatest in this sub-region and this is likely due
513 to wildfire activity in this path in 2003. LJC was heavily burned, and this created a steep slope with few trees
514 that was once moderately to heavily forested. Substantial anchoring and snowfall interception likely created
515 an avalanche path without many large magnitude avalanches for decades since slope forestation plays a
516 substantial role in runout distance and avalanche frequency in forested areas (Teich et al., 2012). In addition,
517 wildfires in 1910 burned a majority of the JFS sub-region as well, and the higher frequency of avalanche
518 years recorded between 1910 and 1940 in S10.7 suggests wildfire impacts may also be a contributor to the
519 high frequency of avalanche events in that location (Reardon et al., 2008). In addition, the fire in LJC may
520 also have removed evidence of previous avalanche activity.

521 Our results also suggest that return interval increases as path length increases, though the sample size for this
522 correlation analysis on individual paths is small (n=12). This result is likely because only very large
523 magnitude avalanches affect the far extent of the runout of the paths. This finding differs from a group of
524 avalanche paths in Rogers Pass, British Columbia, Canada, where path length was not significantly correlated
525 with avalanche frequency (Smith and McClung, 1997). However, that study used all observed avalanches,
526 including artillery-initiated avalanches, as opposed to a tree-ring reconstructed dataset.

527 The greatest number of identified avalanche years is in the JFS sub-region. The avalanche paths in this sub-
528 region are all south or southeasterly facing whereas the other sub-regions span a greater range of aspects.
529 This narrow range of aspect may cause a bias toward overrepresentation of those aspects compared to the
530 inclusion of other aspects in other sub-regions.
531 The differences between individual avalanche paths as well as sub-regions are likely due to localized terrain
532 and weather/climate factors and the interaction of the two (Chesley-Preston, 2010) as well as local avalanche,
533 forest stand, and fire history. For example, Birkeland (2001) demonstrated significant variability of slope
534 stability across a small mountain range dependent upon terrain and weather. Slope stability and subsequent
535 large magnitude avalanching are likely to be highly heterogeneous across not only the sub-region, but across
536 a large region. This is also consistent with findings by Schweizer et al. (2003) that suggest substantial
537 differences in stability between sub-regions despite the presence of widespread weak layers. Finally, climate
538 drives weather, but is not a first order effect on avalanche occurrence in any one given avalanche path. In
539 this study, we derived a regional avalanche chronology to provide a spatial scale that aligns more with the
540 spatial scale of climate drivers than any one individual path. These are relationships that should be examined
541 in future work.

542 **4.3 Regional Chronologies and RAAI**

543 The regional chronology we developed through the use of tree-ring analysis on collections made across 12
544 avalanche paths suggests, unsurprisingly, that the inclusion of more avalanche paths across a large spatial
545 extent produces a more robust identification of major avalanche winters. When we aggregate all 12 paths
546 together and apply thresholds to discriminate the signal from the noise, we identified 30 avalanche years
547 throughout the region. This type of analysis allows us to place each avalanche year in context of the region,
548 or full extent of the scale triplet, rather than simply collating all major avalanche winters identified in each
549 individual path or sub-region. However, we also account for the support and spacing by including adjacent
550 avalanche paths within a sub-region and multiple sub-regions throughout the region. This sampling strategy
551 combined with the large sample size collected throughout the region allowed for a robust assessment of
552 regional avalanche chronology derived from tree-ring records.

553 We tested the sensitivity of the term regional by removing specific and random paths. Our results suggest
554 that removing paths from this structure, and subsequently compromising the sampling strategy, introduces
555 noise. By reducing the sample size, we reduce the ability of the thresholds to filter out noise, thereby
556 increasing the actual number of avalanche years in the region. However, the sample size reduction also
557 reduces the number of identified avalanche winters common to the full 12 path regional record (Table 6).
558 Our results emphasize the importance of sampling more paths spread throughout the region of interest as well
559 as a large dataset across the spatial extent.

560 Avalanche path selection is clearly important when trying to assess avalanche frequency (de Bouchard
561 d'Aubeterre et al., 2019). The importance of path selection is supported by our results suggesting that S10.7
562 is more influential than any other path in our study (Table 6) and is also illustrated by the large number of

563 avalanche years detected in S10.7 due to increased sampling in the track. However, by selecting multiple
564 paths representative of the range of geomorphic and potentially influential local weather controls throughout
565 the region we are able to provide a reasonable assessment of regional avalanche activity in areas without
566 historical records. By quantifying the sensitivity of the number of avalanche paths within a given region, we
567 illustrate that sampling a greater number of avalanche paths dramatically increases the probability of
568 identifying more avalanche years as well as increases the ability to reconstruct major widespread avalanche
569 events. However, as previously noted, dendrochronological techniques tend to underestimate avalanche
570 frequency, which implies that caution should be used when interpreting a regional avalanche signal using
571 this technique, particularly as sample numbers and qualities (e.g. cores vs. cross sections) decline.
572 Interestingly, the difference in median return interval throughout the “region” using 12 paths compared to
573 using four or eight paths changes only slightly suggesting that fewer paths are still able to represent the major
574 avalanche return intervals across a region. However, choosing fewer paths appears to introduce more noise
575 and therefore fewer years identified than a regional chronology with more avalanche paths.
576 The RAAI provides a measure of avalanche activity scaled to the number of active avalanche paths across
577 the region through time, but RAAI is limited by the decreasing sample size back in time. The years with the
578 greatest RAAI value coincide with substantial activity provided in the historical record as well as previous
579 dendrochronological studies from the JFS sub-region (Butler and Malanson, 1985a, b; Reardon et al., 2008).
580 The winter of 1932-33 was characterized by heavy snowfall and persistent cold temperatures leading to
581 extensive avalanche activity that destroyed roadway infrastructure in the JFS sub-region, 1950 saw a nearly
582 month-long closure of U.S. Highway 2 due to avalanche activity, and in 2002, an avalanche caused a train
583 derailment. While these are all confined to the JFS sub-region, with the exception of 2002, they are also years
584 shared by at least two other sub-regions.
585 We examined the probability of detecting an avalanche year throughout the region by sampling any one given
586 path. In seven of 30 years, the POD_{year} is only 8% and in all but three years the POD_{year} is less than 40%. The
587 low POD values are distributed throughout the time series, suggesting decreasing sample size back in time
588 or the number of active avalanche paths is not an influential factor. The POD is likely reflective of the spatial
589 variability of large magnitude avalanche occurrence across a region. It also aligns with the observational
590 findings of Mears (1992). During a major storm in 1986 throughout much of the western United States that
591 deposited 30-60 cm of snow water equivalent, Mears (1992) reported that in the area around Gothic,
592 Colorado, less than 40% of avalanche paths produced avalanches and less than 10% produced avalanches
593 approaching the 100-year return interval. This finding also supports the wide variability of avalanche years
594 between sub-regions recorded in our tree-ring record. Additionally, some of the avalanches in a given year
595 may not be large enough to be reflected in the tree ring record. Therefore, low values of POD_{path} when
596 considering only one avalanche path and identifying only one common year of large magnitude avalanche
597 activity (1982) amongst the sub-regions through dendrochronology is not surprising. The WF sub-region
598 captured the regional chronology most consistently because of the similar and consistent records within the
599 sub-region. Paths with at least one GD (i.e. without applying thresholds) during avalanche years identified in

600 the regional chronology exhibit a greater POD_{path} , but this greater POD_{path} comes at the expense of
601 introducing more noise if we were to simply use one scar per path to define an avalanche event.
602 Our results also suggest that our sampling design using scale triplet increases the probability of detecting
603 avalanche activity across an entire region. We note that we are only able to scale our probability calculations
604 to our dataset with a limited historical observational record. However, our results illustrate the importance of
605 sampling more paths if the goal is to reconstruct a regional chronology. In our dataset, the greatest value of
606 POD_{path} is 40%, suggesting that if by chance, we sampled this path, we would have captured the regional
607 avalanche activity 40% of the time.

608 **4.4 Limitations**

609 Overall, our results suggest that sampling one path, or multiple paths in one sub-region, is insufficient to
610 extrapolate avalanche activity beyond those paths. Multiple paths nested within sub-regions are necessary to
611 glean information regarding avalanche activity throughout those sub-regions as well as the overall region.
612 Our study is still limited by the underrepresentation inherent in dendrochronological techniques for
613 identifying all avalanche events. While we analyzed 673 samples over the extent of the region, some of the
614 paths in our study had relatively small sample sizes per individual path as compared to recent suggestions
615 (Corona et al., 2012). This may have influenced the number of avalanche years identified and subsequent
616 return intervals per individual path. However, we attempted to limit the influence of sample size by using
617 full cross-sections from trees, robust and critical identification of responses in the tree-rings, and appropriate
618 established threshold techniques.
619 We also recognize that sampling more avalanche paths in our region would certainly provide a more robust
620 regional avalanche chronology, but time, cost, and resource constraints required an optimized strategy.
621 Finally, our study would undoubtedly have benefited from a longer and more accurate historical record for
622 comparisons and verification of the tree-ring record in all of the sub-regions. Overall, our study illustrates
623 the importance of considering spatial scale and extent when designing, and making inferences from, regional
624 avalanche studies using tree-ring records.

625 **5. Conclusions**

626 We developed a large magnitude avalanche chronology using dendrochronological techniques for a region
627 in the northern U.S. Rocky Mountains. Implementing a strategic sampling design allowed us to examine
628 avalanche activity through time in single avalanche paths, four sub-regions, and throughout the region. By
629 analyzing 673 samples from 12 avalanche paths, we identified 30 years with large magnitude events across
630 the region and a median return interval of ~ 3 years (from 1866-2017). Large magnitude avalanche return
631 interval and number of avalanche years vary throughout the sub-regions, suggesting the importance of local
632 terrain and weather factors. Our work emphasizes the importance of sample size, scale, and spatial extent
633 when attempting to derive a regional large magnitude avalanche chronology from tree-ring records. In our

634 dataset, the greatest value of POD_{path} is 40%, suggesting that if we sampled only this path, we would have
635 captured the regional avalanche activity 40% of the time. This clearly demonstrates that a single path cannot
636 provide a reliable regional avalanche chronology. Specifically, our results emphasize the importance of 1)
637 sampling more paths spread throughout the region of interest; 2) collecting a large number of cross-sections
638 relative to cores; and, 3) generating a large dataset that scales to the appropriate spatial extent. Future work
639 should include conducting a similar study with a number of paths in the same sub-regions for verification, or
640 in an area with a more robust regional historical record for verification.
641

642 **6. Appendix A**

643 **Table A1: List of previous avalanche-dendrochronological work with more than one avalanche path in study – to**
 644 **place our regional work in context with other regional/multiple path studies. Number of samples, paths, growth**
 645 **disturbances (GD), and spatial extent (linear distance between most distant avalanche paths in study area) are**
 646 **included. For spatial extent, NA is reported in studies where spatial extent is not reported or could not be inferred**
 647 **from maps in the published work. Where spatial extent is not reported directly in previous work, it is estimated**
 648 **by using maps from the published work and satellite imagery. We included only the initial studies using a dataset**
 649 **with more than one avalanche path. For example, if a study used the same dataset again in subsequent work, we**
 650 **did not include it.**

Authors	Location	# Trees	# Samples	# Paths	Spatial Extent	# GD
Gratton et al. (2019)	Northern Gaspé Peninsula, Québec, Canada	82	177 cores 65 x- sec	5	~20 km	Not provided
Meseşan et al. (2018)	Parâng Mountains, Carpathians, Romania	232	430 cores 39 x-sec 4 wedges	3	~16 km	Not provided
Favillier et al. (2018)	Zermatt valley, Switzerland	307	620 cores 60 x-sec	3	~1 km	2570
Ballesteros-Canovas (2018)	Kullu district, Himachal Pradesh, India	114	Not Provided	1 slope (multiple paths)	~ 1 km	521
Pop et al.(2018)	Piatra Craiului Mountains, Romania	235	402 cores 34 x-sec	2	~ 2 km	789
Martin and Germain (2016)	White Mountains, New Hampshire	450	350 cores 456 x-sec	7	~10 km	2251
Voiculescu et al. (2016)	Făgăras massif, Carpathians, Romania	293	586 cores	4	NA	853
Schläppy et al. (2015)	French Alps, France	967	1643 cores 333 x-sec	5	~100 km	3111
Schläppy et al. (2014)	French Alps, France	297	375 cores 63 x-sec	2	~100 km	713
Schläppy et al. (2013)	French Alps, France	587	1169 cores 122 x-sec	3	~100 km	1742
Casteller et al. (2011)	Santa Cruz, Argentina	95	~95 x-sec	9	~2 km	Not provided

Köse et al. (2010)	Katsomonu, Turkey	61	Not provided	2	~ 500 m	Not provided
Muntán et al. (2009)	Pyrenees, Catalonia	NA	448	6	~150 km	Not provided
Germain et al. (2009)	Northern Gaspé Peninsula, Québec, Canada	689	1214 x-sec	12	~30 km	2540
Butler and Sawyer (2008)	Lewis Range, Glacier National Park, Montana, USA	22	22 x-sec	2	~5 km	Not provided
Casteller et al. (2007)	Grisons, Switzerland	145	122 x-sec 52 cores 10 wedges	2	~ 20 km	Not provided
Germain et al. (2005)	Northern Gaspé Peninsula, Québec, Canada	142	142 x-sec	5	NA	420
Dube et al.(2004)	Northern Gaspé Peninsula, Québec, Canada	110	170 x-sec	3	~9 km	Not provided
Hebertson and Jenkins (2003)	Wasatch Plateau, Utah, USA	261	Not provided	16	NA	Not provided
Rayback (1998)	Front Range, Colorado, USA	98	58 trees cored (2-5 cores /tree) 31 x-sec 9 wedges	2	~7 km	Not provided
Bryant et al. (1989)	Huerfano Valley, Colorado, USA	180	Not provided	3	~2 km	Not provided
Butler and Malanson (1985a)	Lewis Range, Glacier National Park, Montana, USA	78	Not provided	2	~6 km	Not provided
Butler (1979)~	Glacier National Park, Montana, USA	NA	36 x-sec 17 cores	12	~15 km	Not provided
Smith (1973)	North Cascades, Washington, USA	NA	Not provided	11	~ 35 km	Not provided
Potter (1969)	Absaroka Mountains, Wyoming, USA	50	Not provided	5	~ 2 km	50

652 **Table A2: Regional chronologies from the International Tree-Ring Database used for cross-dating.**

MT Avalanche Project Site	ITRDB Tree-Ring Chron.	Originator	Date Range	Species	Coordinates	Elevation	NOAA set ID	data
Going-to-the-Sun Road sites	Going to the Sun Road (GTS)	Gregory T. Pederson Jeremy S. Littell	1337 - 2002	PSME	48.42 -113.5167	1860M	noaa-tree-27540_MT159	
John F. Stevens Canyon sites	Doody Mountain (DOO)	Gregory T. Pederson Blase Reardon	1660 - 2001	PSME	48.3833 -113.6167	1890M	noaa-tree-27536_MT155	
Lost Johnny Creek sites	Preston Park (PP)	Bekker, M.F.; Tikalsky, B.P.; Fagre, D.B.; Bills, S.D.	1766 - 2006	ABLA	48.43 -113.39	2150M	noaa-tree-5993_MT117	
Red Meadow sites	Numa Ridge Falls (NRF)	Gregory T. Pederson Brian Peters	1645 - 2001	PSME	48.51 -114.12	1695M	noaa-tree-27550_MT168	

653
654 **Table A3: Proportion of input types (tree-ring signals) to each growth disturbance (GD) class. Note that there**
655 **could be multiple input types for each class. Termination of growth indicates that the tree was killed in that year**
656 **and it coincides with the historical avalanche record. Some of the termination of growth samples have earlywood**
657 **if the avalanche occurred in the late winter or early spring. Refer to Table 3 for definitions of classes.**

Type	C ₁	C ₂	C ₃	C ₄	C ₅
Scar	0.37	0.10	0.04	0.01	0.00
Reaction Wood	0.16	0.59	0.66	0.67	0.64
Growth Suppression	0.05	0.15	0.17	0.23	0.27
Traumatic Resin Ducts	0.17	0.16	0.12	0.09	0.08
Termination of Growth	0.25	0.00	0.00	0.00	0.00

658
659 **Table A4: Summary data of subset of samples (n=40) used to estimate number of GDs potentially missed if core**
660 **were analyzed instead of the entire cross-section.**

# trees	40
# original GDs	191
Missed C1	24
Missed C2	24
Missed C3	14
Missed C4	3
Missed C5	2
Total # years missed by cores	67
% of GDs missed	35
Total # years ID'd by cores that were in x-sec	124
% captured by cores	65

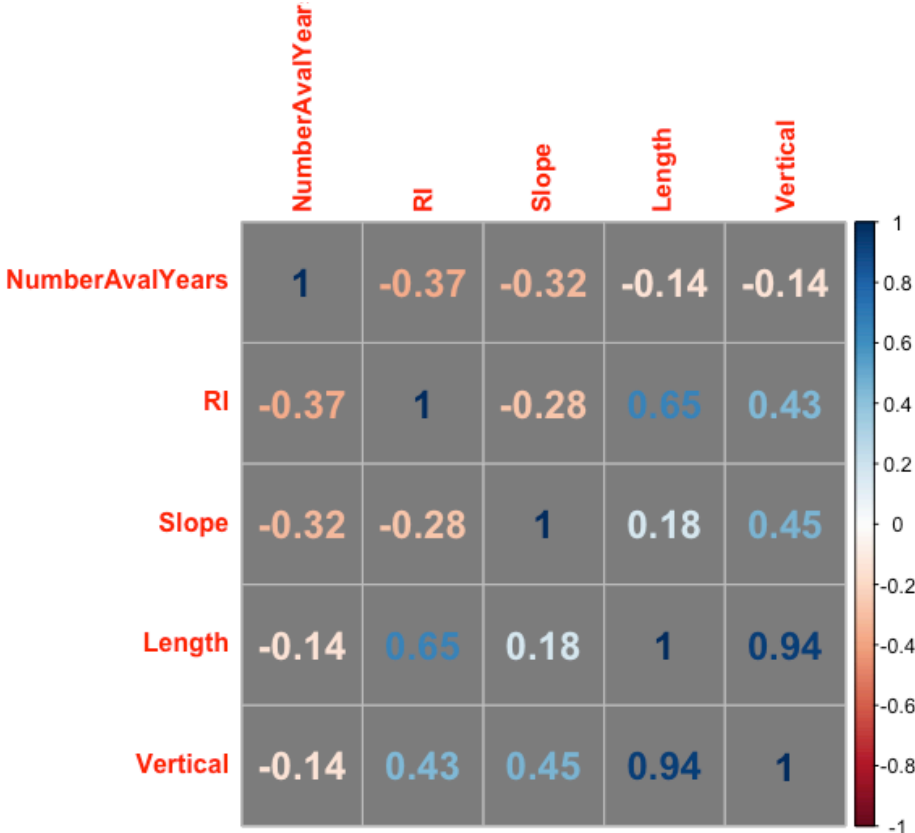
661

662 Table A5: Avalanche Years identified in the regional analysis (Region, n=29) and avalanche years identified in
663 one or more paths in the individual avalanche path analysis (Paths Unique Years, n=49). Years in bold indicate
664 years in common between the two sets (n=27).

Region	Paths Unique Years
1866	1866
1872	1872
1880	1880
	1907
	1912
	1913
	1923
1933	1933
1936	1936
	1943
1945	
1948	1948
	1949
1950	1950
1954	1954
1956	
1965	1965
	1966
	1967
	1968
1970	1970
1971	1971
1972	1972
1974	1974
1976	1976
	1979
1982	1982
	1983
	1985
	1986
	1987
	1989
1990	1990
	1991
	1992
1993	1993
	1995
	1996
1997	1997
1998	1998
	1999

	2001
2002	2002
2003	2003
2004	2004
2009	2009
	2010
2011	2011
2012	2012
2014	2014
2017	2017

665



666

667 **Figure A1: Correlation matrix (Pearson correlations coefficients) of the number of avalanche years, return**
 668 **interval (RI), starting zone slope angle (Slope), and path length (Length). Statistical significance is $p < 0.05$. See**
 669 **source data in Table 1.**

670 **7. Data availability**

671 Data for this work can be found in ScienceBase repository: Peitzsch, E. H., Stahle, D. K., Fagre, D. B., Clark,
 672 A. M., Pederson, G. T., Hendrikx, J., and Birkeland, K. W.: Tree ring dataset for a regional avalanche
 673 chronology in northwest Montana, 1636-2017. U.S. Geological Survey., U.S. Geological Survey data release,
 674 <https://doi.org/10.5066/P9TLHZAI>, 2019.

675 **8. Author contribution**

676 EP responsible for study conception and design, data collection, analysis, writing. JH contributed to
677 development of study design, methods, editing, and writing. DS responsible for data collection, tree-ring
678 processing and analysis and writing. GP, KB, and DF contributed to study design, editing and writing.

679 **9. Disclaimer**

680 Any use of trade, firm, or product names is for descriptive purposes only and does not imply endorsement by
681 the U.S. Government.

682 **10. Acknowledgements**

683 We extend gratitude to Adam Clark for his substantial data collection efforts and Zach Miller for his
684 assistance processing samples. This work was supported by the U.S. Geological Survey Land Resources
685 Western Mountain Initiative project.

686 **11. References**

687 Armstrong, B. R.: A quantitative analysis of avalanche hazard on U.S. Highway 550, southwestern Colorado,
688 in: Proceedings of the Western Snow Conference, St. George, Utah, April 14-16, 2017, 95-104, 1981.

689

690 Ballesteros-Canovas, J. A., Trappmann, D., Madrigal-Gonzalez, J., Eckert, N., and Stoffel, M.: Climate
691 warming enhances snow avalanche risk in the Western Himalayas, Proc. Natl. Acad. Sci. U.S.A., 115, 3410-
692 3415, [10.1073/pnas.1716913115](https://doi.org/10.1073/pnas.1716913115), 2018.

693

694 Bebi, P., Kulakowski, D., and Rixen, C.: Snow avalanche disturbances in forest ecosystems-State of research
695 and implications for management, For. Ecol. and Manage., 257, 1883-1892, [10.1016/j.foreco.2009.01.050](https://doi.org/10.1016/j.foreco.2009.01.050),
696 2009.

697

698 Birkeland, K. W.: Spatial patterns of snow stability throughout a small mountain range, J. Glaciol., 47, 176-
699 186, [10.3189/172756501781832250](https://doi.org/10.3189/172756501781832250) 2001.

700

701 Blöschl, G., and Sivapalan, M.: Scale issues in hydrological modelling: A review, Hydrol. Processes, 9, 251-
702 290, [10.1002/hyp.3360090305](https://doi.org/10.1002/hyp.3360090305) 1995.

703

704 Blöschl, G.: Scaling issues in snow hydrology, Hydrol. Processes, 13, 2149-2175, [10.1002/\(SICI\)1099-
705 1085\(199910\)13:14/15%3C2149::AID-HYP847%3E3.0.CO;2-8](https://doi.org/10.1002/(SICI)1099-1085(199910)13:14<15%3C2149::AID-HYP847%3E3.0.CO;2-8), 1999.

706

707 Bryant, C.L., Butler, D.R., Vitek, J.D.: A statistical analysis of tree-ring dating in conjunction with snow
708 avalanches – comparison of on-path versus off-path responses, *Environ. Geol. Water Sci.*, 14, 53-59,
709 10.1007/BF01740585, 1989.

710

711 Burrows, C. J., and Burrows, V. L.: Procedures for the study of snow avalanche chronology using growth
712 layers of woody plants, Institute of Arctic and Alpine Research, University of Colorado, Boulder, CO,
713 Occasional Paper No. 23, 56 pp., 1976.

714

715 Butler, D. R.: Snow avalanche path terrain and vegetation, Glacier National Park, Montana, *Arc. and Alp.*
716 *Res.*, 11, 17-32, [10.1080/00040851.1979.12004114](https://doi.org/10.1080/00040851.1979.12004114), 1979.

717

718 Butler, D. R., and Malanson, G., P.: A history of high-magnitude snow avalanches, southern Glacier National
719 Park, Montana, U.S.A., *Mt. Res. Dev.*, 5, 175-182, 10.2307/3673256, 1985a.

720

721 Butler, D. R., and Malanson, G. P.: A reconstruction of snow-avalanche characteristics in Montana, U.S.A.,
722 using vegetative indicators, *J. of Glaciol.*, 31, 185-187, [10.3189/S0022143000006444](https://doi.org/10.3189/S0022143000006444), 1985b.

723

724 Butler, D. R., Malanson, G. P., and Oelfke, J. G.: Tree-ring analysis and natural hazard chronologies:
725 minimum sample sizes and index values, *Prof. Geogr.*, 39, 41-47, [10.1111/j.0033-0124.1987.00041.x](https://doi.org/10.1111/j.0033-0124.1987.00041.x), 1987.

726

727 Butler, D. R., and Sawyer, C. F.: Dendrogeomorphology and high-magnitude snow avalanches: a review and
728 case study, *Nat. Hazard Earth Sys.*, 8, 303-309, 10.5194/nhess-8-303-2008, 2008.

729

730 Colorado Avalanche Information Center Statistics and Reporting.
731 <http://avalanche.state.co.us/accidents/statistics-and-reporting/>, last access: June 8, 2020.

732

733 Carrara, P. E.: The determination of snow avalanche frequency through tree-ring analysis and historical
734 records, *Geol. Soc. Am. Bull.*, 90, 773-780, [10.1130/0016-7606\(1979\)90%3C773:TDOSAF%3E2.0.CO;2](https://doi.org/10.1130/0016-7606(1979)90%3C773:TDOSAF%3E2.0.CO;2),
735 1979.

736

737 Casteller, A., Stoeckli, V., Villalba, R., Mayer, A.C.: An evaluation of dendroecological indicators of snow
738 avalanches in the Swiss Alps, *Arct. Antarct. Alp. Res.*, 39, 218-228, [10.1657/1523-
739 0430\(2007\)39\[218:AEODIO\]2.0.CO;2](https://doi.org/10.1657/1523-0430(2007)39[218:AEODIO]2.0.CO;2), 2007.

740

741 Casteller, A., Villalba, R., Araneo, D., and Stöckli, V.: Reconstructing temporal patterns of snow avalanches
742 at Lago del Desierto, southern Patagonian Andes, *Cold Reg. Sci. Technol.*, 67, 68-78,
743 10.1016/j.coldregions.2011.02.001, 2011.

744

745 Chesley-Preston, T.: Patterns of natural avalanche activity associated with new snow water equivalence and
746 upper atmospheric wind direction and speed in the mountains surrounding Gothic, Colorado, Master of
747 Science, Department of Earth Sciences, Montana State University, Bozeman, Montana, 75 pp., 2010.

748

749 Corona, C., Lopez Saez, J., Stoffel, M., Bonnefoy, M., Richard, D., Astrade, L., and Berger, F.: How much
750 of the real avalanche activity can be captured with tree rings? An evaluation of classic dendrogeomorphic
751 approaches and comparison with historical archives, *Cold Reg. Sci. Technol.*, 74-75, 31-42,
752 10.1016/j.coldregions.2012.01.003, 2012.

753

754 de Bouchard d'Aubeterre, G., Favillier, A., Mainieri, R., Lopez Saez, J., Eckert, N., Saulnier, M., Peiry, J. L.,
755 Stoffel, M., and Corona, C.: Tree-ring reconstruction of snow avalanche activity: Does avalanche path
756 selection matter?, *Sci. Total Environ.*, 684, 496-508, 10.1016/j.scitotenv.2019.05.194, 2019.

757

758 Dube, S., Filion, L., and Hetu, B.: Tree-Ring Reconstruction of High-Magnitude Snow Avalanches in the
759 Northern Gaspé Peninsula, Quebec, Canada, *Arct. Antarct. Alp. Res.*, 36, 555-564, [10.1657/1523-
760 0430\(2004\)036\[0555:TROHSA\]2.0.CO;2](https://doi.org/10.1657/1523-0430(2004)036[0555:TROHSA]2.0.CO;2), 2004.

761

762 Favillier, A., Guillet, S., Morel, P., Corona, C., Lopez Saez, J., Eckert, N., Ballesteros Cánovas, J. A., Peiry,
763 J.-L., and Stoffel, M.: Disentangling the impacts of exogenous disturbances on forest stands to assess multi-
764 centennial tree-ring reconstructions of avalanche activity in the upper Goms Valley (Canton of Valais,
765 Switzerland), *Quat. Geochronol.*, 42, 89-104, 10.1016/j.quageo.2017.09.001, 2017.

766

767 Favillier, A., Guillet, S., Trappmann, D., Morel, P., Lopez-Saez, J., Eckert, N., Zenhäusern, G., Peiry, J.-L.,
768 Stoffel, M., and Corona, C.: Spatio-temporal maps of past avalanche events derived from tree-ring analysis:
769 A case study in the Zermatt valley (Valais, Switzerland), *Cold Reg. Sci. Technol.*, 154, 9-22,
770 10.1016/j.coldregions.2018.06.004, 2018.

771

772 Germain, D., Filion, L., and Héту, B.: Snow avalanche activity after fire and logging disturbances, northern
773 Gaspé Peninsula, Quebec, Canada, *Can. J. of Earth Sci.*, 42, 2103-2116, 10.1139/e05-087, 2005.

774

775 Germain, D., Filion, L., and Héту, B.: Snow avalanche regime and climatic conditions in the Chic-Choc
776 Range, eastern Canada, *Clim. Change*, 92, 141-167, 10.1007/s10584-008-9439-4, 2009.

777

778 Germain, D., Héту, B., and Filion, L.: Tree-ring based reconstruction of past snow avalanche events and risk
779 assessment in Northern Gaspé Peninsula (Québec, Canada), in: *Tree Rings and Natural Hazards - A State-*

780 of-the-Art, edited by: Stoffel, M., Bollschweiler, M., Butler, D. R., and Luckman, B. H., *Advances in Global*
781 *Change Research*, Springer, London, 51-73, 2010.

782

783 Google. (n.d.). [Imagery of study area, northwest Montana]. Retrieved February 4, 2020 using R statistical
784 package `get_map`.

785

786 Gratton, M., Germain, D., and Boucher, É.: Meteorological triggering scenarios of tree-ring-based snow
787 avalanche occurrence on scree slopes in a maritime climate, Eastern Canada, *Phys. Geogr.*, 1-18,
788 10.1080/02723646.2019.1573622, 2019.

789

790 Greene, E., Birkeland, K. W., Elder, K., McCammon, I., Staples, M., and Sharaf, D.: *Snow, weather, and*
791 *avalanches: Observation guidelines for avalanche programs in the United States (3rd ed)*, American
792 *Avalanche Association*, Victor, ID, 104 pp., 2016.

793

794 Grissino-Mayer, H.: Evaluating crossdating accuracy: A manual and tutorial for the computer
795 program COFECHA, *Tree-Ring Res.*, 57, 205-221, 2001.

796

797 Hebertson, E. G., and Jenkins, M. J.: Historic climate factors associated with major avalanche years on the
798 Wasatch Plateau, Utah, *Cold Reg. Sci. Technol.*, 37, 315-332, 10.1016/S0165-232x(03)00073-9, 2003.

799

800 Hendrikx, J., Murphy, M., and Onslow, T.: Classification trees as a tool for operational avalanche forecasting
801 on the Seward Highway, Alaska, *Cold Reg. Sci. and Technol.*, 97, 113-120,
802 10.1016/j.coldregions.2013.08.009, 2014.

803

804 Holmes, R. L.: Analysis of tree rings and fire scars to establish fire history, *Tree-Ring Bulletin*, 43, 51-67,
805 1983.

806

807 International Tree Ring Data Bank (ITRDB): [https://www.ncdc.noaa.gov/data-access/paleoclimatology-](https://www.ncdc.noaa.gov/data-access/paleoclimatology-data/datasets/tree-ring)
808 [data/datasets/tree-ring](https://www.ncdc.noaa.gov/data-access/paleoclimatology-data/datasets/tree-ring), access: March 1, 2018.

809

810 Kogelnig-Mayer, B., Stoffel, M., Schneuwly-Bollschweiler, M., Hübl, J., and Rudolf-Miklau, F.:
811 Possibilities and Limitations of Dendrogeomorphic Time-Series Reconstructions on Sites Influenced by
812 Debris Flows and Frequent Snow Avalanche Activity, *Arct. Antarct. Alp. Res.*, 43, 649-658, 10.1657/1938-
813 4246-43.4.649, 2011.

814

815 Korpela, M., Wickham, H., Jackson, S. *ggmap v3.0.0 – Spatial Visualization with ggplot2*.
816 <https://github.com/dkahle/ggmap>. 2019.

817

818 Köse, N., Aydın, A., Akkemik, Ü., Yurtseven, H., and Güner, T.: Using tree-ring signals and numerical
819 model to identify the snow avalanche tracks in Kastamonu, Turkey, *Nat. Hazards*, 54, 435-449,
820 10.1007/s11069-009-9477-x, 2010.

821

822 Malevich, S. B., Guiterman, C. H., and Margolis, E. Q.: burnr : Fire history analysis and graphics in R,
823 *Dendrochronologia*, 49, 9-15, 10.1016/j.dendro.2018.02.005, 2018.

824

825 Martin, J. P., and Germain, D.: Dendrogeomorphic reconstruction of snow avalanche regime and triggering
826 weather conditions: A classification tree model approach, *Prog. Phys. Geog.*, 10.1177/0309133315625863,
827 2016.

828

829 Mears, A. I.: Snow-Avalanche Hazard Analysis for Land-use Planning and Engineering, Colorado
830 Geological Survey Bulletin, 49, 55 pp., 1992.

831

832 Meseşan, F., Gavrilă, I. G., and Pop, O. T.: Calculating snow-avalanche return period from tree-ring data,
833 *Nat. Hazards*, 94, 1081-1098, 10.1007/s11069-018-3457-y, 2018.

834

835 Mock, C. J., and Birkeland, K. W.: Snow avalanche climatology of the western United States mountain
836 ranges, *Bull. Am. Meteorol. Soc.*, 81, 2367-2392, [10.1175/1520-
837 0477\(2000\)081%3C2367:SACOTW%3E2.3.CO;2](https://doi.org/10.1175/1520-0477(2000)081%3C2367:SACOTW%3E2.3.CO;2), 2000.

838

839 Mock, C. J., Carter, K. C., and Birkeland, K. W.: Some Perspectives on Avalanche Climatology, *Ann. Am.*
840 *Assoc. of Geogr.*, 1-10, 10.1080/24694452.2016.1203285, 2016.

841

842 Muntán, E., Garcia, C., Oller, P., Marti, G., Garcia, A., and Gutierrez, E.: Reconstructing snow avalanches
843 in the Southeastern Pyrenees, *Nat. Hazard Earth Sys.*, 9, 1599-1612, 10.5194/nhess-9-1599-2009, 2009.

844

845 Ott, R. L., and Longnecker, M. T.: *An Introduction to Statistical Methods and Data Analysis*, 7th Edition ed.,
846 Cengage Learning, Boston, MA, 1296 pp., 2016.

847

848 Peitzsch, E. H., Stahle, D. K., Fagre, D. B., Clark, A. M., Pederson, G. T., Hendrikx, J., and Birkeland, K.
849 W.: Tree ring dataset for a regional avalanche chronology in northwest Montana, 1636-2017. U.S. Geological
850 Survey., U.S. Geological Survey data release, 10.5066/P9TLHZAI, 2019.

851

852 Pop, O. T., Munteanu, A., Flaviu, M., Gavrilă, I.-G., Timofte, C., and Holobăcă, I.-H.: Tree-ring-based
853 reconstruction of high-magnitude snow avalanches in Piatra Craiului Mountains (Southern Carpathians,

854 Romania), *Geografiska Annaler: Series A, Phys. Geogr.*, 100, 99-115, 10.1080/04353676.2017.1405715,
855 2018.
856

857 Potter, N.: Tree-ring dating of snow avalanche tracks and the geomorphic activity of avalanches, Northern
858 Absaroka Mountains, Wyoming, *Geol. S. Am. S., Special Paper 123*, 141-165, 1969.
859

860 Rayback, S. A.: A dendrogeomorphological analysis of snow avalanches in the Colorado Front Range, USA,
861 *Phys. Geogr.*, 19, 502-515, [10.1080/02723646.1998.10642664](https://doi.org/10.1080/02723646.1998.10642664), 1998.
862

863 Reardon, B. A., Pederson, G. T., Caruso, C. J., and Fagre, D. B.: Spatial reconstructions and comparisons of
864 historic snow avalanche frequency and extent using tree rings in Glacier National Park, Montana, U.S.A.,
865 *Arct. Antarct. Alp. Res.*, 40, 148-160, 10.1657/1523-0430(06-069)[REARDON]2.0.CO;2, 2008.
866

867 Schläppy, R., Jomelli, V., Grancher, D., Stoffel, M., Corona, C., Brunstein, D., Eckert, N., and Deschatres,
868 M.: A New Tree-Ring-Based, Semi-Quantitative Approach for the Determination of Snow Avalanche
869 Events: use of Classification Trees for Validation, *Arct. Antarct. Alp. Res.*, 45, 383-395, 10.1657/1938-4246-
870 45.3.383, 2013.
871

872 Schläppy, R., Eckert, N., Jomelli, V., Stoffel, M., Grancher, D., Brunstein, D., Naaim, M., and Deschatres,
873 M.: Validation of extreme snow avalanches and related return periods derived from a statistical-dynamical
874 model using tree-ring techniques, *Cold Reg. Sci. Technol.*, 99, 12-26, 10.1016/j.coldregions.2013.12.001,
875 2014.
876

877 Schläppy, R., Jomelli, V., Eckert, N., Stoffel, M., Grancher, D., Brunstein, D., Corona, C., and Deschatres,
878 M.: Can we infer avalanche–climate relations using tree-ring data? Case studies in the French Alps, *Reg.*
879 *Environ. Change*, 16, 629-642, 10.1007/s10113-015-0823-0, 2015.
880

881 Schweizer, J.: Snow avalanche formation, *Reviews of Geophysics*, 41, 10.1029/2002rg000123, 2003.
882

883 Schweizer, J., Kronholm, K., and Wiesinger, T.: Verification of regional snowpack stability and avalanche
884 danger, *Cold Reg. Sci. and Technol.*, 37, 277-288, 10.1016/s0165-232x(03)00070-3, 2003.
885

886 Selkowitz, D. J., Fagre, D. B., and Reardon, B. A.: Interannual variations in snowpack in the Crown of the
887 Continent Ecosystem, *Hydrol. Process.*, 16, 3651-3665, 10.1002/hyp.1234, 2002.
888

889 Shroder, J. F.: Dendrogeomorphological analysis of mass movement on Table Cliffs Plateau, Utah,
890 *Quaternary Res.*, 9, 168-185, 10.1016/0033-5894(78)90065-0, 1978.

891

892 Šilhán, K., and Tichavský, R.: Snow avalanche and debris flow activity in the High Tatras Mountains: New
893 data from using dendrogeomorphic survey, *Cold Reg. Sci. Technol.*, 134, 45-53,
894 10.1016/j.coldregions.2016.12.002, 2017.

895

896 Skøien, J. O., and Blöschl, G.: Sampling scale effects in random fields and implications for environmental
897 monitoring, *Environ. Monit. Assess.*, 114, 521-552, 10.1007/s10661-006-4939-z, 2006.

898

899 Smith, L.: Indication of snow avalanche periodicity through interpretation of vegetation patterns in the North
900 Cascades, Washington , in: *Methods of Avalanche Control on Washington Mountain Highways: Third*
901 *Annual Report*, Washington State Highway Commission Department of Highways, Olympia, Washington,
902 USA, 187 pp., 1973.

903

904 Smith, M. J., and McClung, D. M.: Avalanche frequency and terrain characteristics at Rogers' pass, British
905 Columbia, Canada, *J. Glaciol.*, 43, 165-171, [10.3189/S002214300002926](https://doi.org/10.3189/S002214300002926), 1997.

906

907 Stokes, M. A., and Smiley, T. L.: *An Introduction to Tree-Ring Dating*, The University of Arizona Press,
908 Tucson, 1996.

909

910 Teich, M., Bartelt, P., Grêt-Regamey, A., and Bebi, P.: Snow Avalanches in Forested Terrain: Influence of
911 Forest Parameters, Topography, and Avalanche Characteristics on Runout Distance, *Arct. Antarct. Alp. Res.*,
912 44, 509-519, 10.1657/1938-4246-44.4.509, 2012.

913

914 Voiculescu, M., Onaca, A., and Chiroiu, P.: Dendrogeomorphic reconstruction of past snow avalanche events
915 in Bâlea glacial valley–Făgăraș massif (Southern Carpathians), Romanian Carpathians, *Quatern. Int.*, 415,
916 286-302, 10.1016/j.quaint.2015.11.115, 2016.